Theoretical Methods of Potential Use for Studies of Inorganic Reaction Mechanisms

Tom Ziegler*,† and Jochen Autschbach‡

Department of Chemistry, University of Calgary, 2500 University Drive NW, Calgary T2N 1N4, Canada, and Department of Chemistry, University at Buffalo, State University of New York, 312 Natural Sciences Complex, Buffalo, New York 14260-3000

Received September 6, 2004

Contents

* To whom correspondence should be addressed. Tel: +1-403-220-5368. Fax: +1-403-289-9488. E-mail: Ziegler@ucalgary.ca.
† University of Calgary.
‡ University at Buffalo State University of New York.

1. Introduction

It is customary[1] to analyze a chemical process as a series of several elementary reaction steps. In every elementary step, a transformation takes place from one minimum on the potential energy surface (PES) representing the reactants ($R_1 + R_2$) over an energy maximum (the transition state, TS) to another energy minimum characterized by the products ($P_1 + P_2$). For each elementary step, the identities of products and reactants are determined experimentally along with the reaction rate, k. The analysis of inorganic processes in terms of elementary reaction steps was pioneered after the Second World War with the experimental work by Taube,[1] Basolo,[2] Pearson,[3] and many more.[1]

It is in principle possible by quantum mechanics (QM) to characterize the PES for the elementary reaction step[4] given in eq 1

$$R_1 + R_2 \xrightarrow{k} P_1 + P_2 \qquad (1)$$

as well as the structures of the reactants, products, and TSs. The first use of QM in studies of inorganic elementary reaction steps made use of several simplifying assumptions and only provided rather approximate solutions to the fundamental underlying equations. Best known is perhaps the use of crystal-field theory (CF) to rationalize observed trends in the

10.1021/cr0307188 CCC: $53.50
Published on Web 04/21/2005

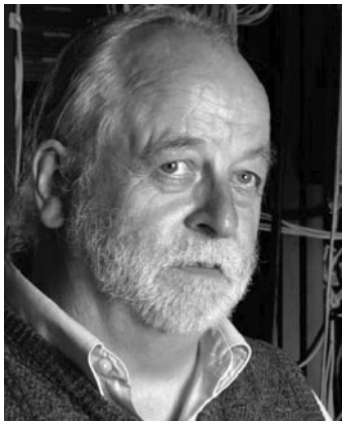

Tom Ziegler was raised in Denmark and graduated from the University of Copenhagen in 1972 with a Cand.Scient degree in theoretical chemistry. He obtained a Ph.D. from the University of Calgary (1978) where he has been a full professor since 1991 and currently is holding a Canada Research Chair in theoretical inorganic chemistry. He has in the last 30 years worked with the development of density functional theory as a practical tool in transition metal chemistry and homogeneous catalysis. This has led to computational methods of use in spectroscopy, thermochemistry, structure determination, and molecular dynamics. He is a fellow of both the Royal Danish Society and the Royal Canadian Society.

Jochen Autschbach (born 1968) received a Ph.D. in theoretical chemistry from the University of Siegen (Germany) in 1999. During three years as a postdoctoral fellow in Tom Ziegler's group in Calgary (Canada), he got interested in calculations of NMR parameters of heavy nuclei and optical activities of transition metal complexes. In 2002, he received an Emmy-Noether fellowship of the Deutsche Forschungsgemeinschaft. Since August 2003, he has been an assistant professor at the State University of New York at Buffalo (United States). His current research interests are the calculation of linear and nonlinear molecular magnetic response properties, solvent and other environmental effects on molecular spectroscopic parameters, and properties of nanoscale materials.

rate of ligand substitution reactions involving transition metal complexes.[1] Other approaches include the perturbational molecular orbital (PMO) theory[5] in which trends in rates are rationalized in terms of symmetry arguments[5] and the hardness[5c] and softness[5c] of the reactive centers on $R_1 + R_2$.

Progress in both theory (software) and computer technology (hardware) has made it feasible over the past 10 years to describe the PES of smaller systems with nearly chemical accuracy (1 kcal/mol). Even larger systems can be described with reasonable computational affords, although the accuracy now is somewhat less (~5 kcal/mol). This development will be reviewed in section 2 where we also discuss how one can include the influence of the solvent and bulky

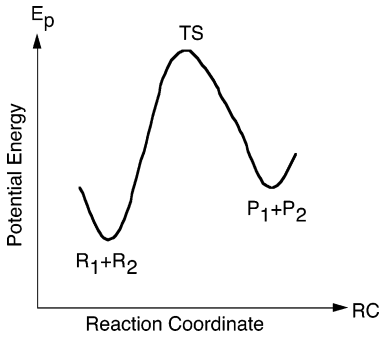

Figure 1. Energy profile for the elementary reaction step $R_1 + R_2 \rightarrow P_1 + P_2$.

substituents on the shape of the potential energy path (Figure 1) of a chemical reaction for both the ground state and the higher lying excited states. It should be pointed out that the qualitative arguments based on PMO as they have been used in the past also should have a future place in rationalizing the results from modern quantitative calculations on chemical systems.

The ability to locate products and reactants on the PES along with the TS structures is one of the more important achievements of computational chemistry. This development is discussed in section 3 together with methods that allow one to trace a minimum energy path (MEP) from reactant over TS to product. This is supplemented in section 4 with a discussion of how one takes steric bulk and solvation effects into account. Section 5 discusses how theoretical methods can be used to explore the PESs of the excited states as well.

One of the most important experimental techniques used to establish information about the species involved in a chemical reaction is spectroscopy. We discuss in section 6 how theoretical methods are able to obtain spectroscopic parameters from first principle for nuclear magnetic resonance (NMR), electron spin resonance (ESR), infrared (IR), and electronic spectroscopy. The potential of supplementing experimental spectroscopy with theoretical calculations in studies of inorganic reaction mechanisms has not been fully explored.

The energy profile in Figure 1 contains only information about the chemical reaction of eq 1 at 0 K whereas the rate constant (k) and the equilibrium between $R_1 + R_2$ and $P_1 + P_2$ are related to the free energy of the system[6] at a finite temperature. Thus, on top of the quantum mechanical calculations generating the PES, we need a statistical treatment that averages over different initial velocities of the atoms in $R_1 + R_2$ for the trajectories leading to the products $P_1 + P_2$. The different statistical methods used to achieve this objective are discussed in section 8. Section 9 looks toward new frontiers in the modeling of inorganic reaction mechanisms with respect to both new method developments and novel applications.

It has not been the objective here to review the large volume of papers dealing with the application of theoretical methods to the study of chemical reactions. It has instead been the intension to review theoretical methods that are already applied, or have

the potential to be applied, to the study of inorganic reaction mechanisms. Special emphasis will be given to the foundation of these methods and their accuracy. The relatively few practical examples given here are not comprehensive. They are mostly chosen to illustrate the use of the methods.

2. PESs and Electronic Structure Theory

We shall in this section discuss the different electronic structure theories used to generate PESs for transition metal complexes and other molecular systems. Special attention will be given to the accuracy one can expect from the different methods.

2.1. First Principle Determination of the PES

A molecular system in a stationary state is fully characterized by the solution Θ to the many-electron Schrödinger equation

$$\hat{H}_T\Theta = E_T\Theta \tag{2}$$

Here, Θ is a wave function that depends on the electronic and nuclear coordinates and $\hat{H}_T$ is the quantum mechanical Hamiltonian[4] of the molecule whereas the factor E_T is the energy of the system. It is a good approximation to consider the motion of the electrons as much faster than the nuclei (the Born−Oppenheimer approximation[4]). In this case, the nuclei can be fixed in space and the Schrödinger equation can be reduced to

$$\hat{H}\Psi = E\Psi \tag{3}$$

Here, E is the potential energy $E(\vec{q}_1,\vec{q}_2,\vec{q}_3,...,\vec{q}_N)$of the molecule at the nuclear coordinates $\{\vec{q}_i, i = 1,N\}$ and $\hat{H}$ is the Hamiltonian of the molecule with the kinetic energy of the nuclei omitted[4] whereas Ψ is a function (the electronic wave function) that depends on the coordinates of the electrons. The PES $E(\vec{q}_1,\vec{q}_2,\vec{q}_3,...,\vec{q}_N)$ can now in principle be obtained from the solution of eq 3 at all nuclear conformations. By expanding Ψ in terms of so-called Slater determinants[4] D_i as

$$\Psi = \sum_{i=1}^{m_o} f_i D_i \tag{4}$$

equation 3 can be solved to any degree of accuracy. Here,

$$D_i = |\varphi_{i1}(1)\ \varphi_{i2}(2)\ \varphi_{i3}(3)...\varphi_{in}(n)| \tag{5}$$

is a determinant with the general element for row k and column j given by the function $\varphi_{ik}(j)$. The index (j) indicates the space and spin coordinates of electron j. The function $\varphi_{ik}(j)$ is in turn expressed as a linear combination of a set of known functions $\{\chi_r; r = 1,m\}$ as

$$\varphi_{ik}(j) = \sum_{r=1}^{r=m} C_{ik,r}\,\chi_r(j) \tag{6}$$

In practical calculations, $\{\chi_r; r = 1,m\}$ is a set of atomic orbitals and the corresponding molecular orbitals $\varphi_{ik}(j)$ are thus written as a linear combination of atomic orbitals. The coefficients f_i and $C_{ik,r}$ of eqs 4 and 6, respectively, are determined in such a way as to minimize[4] the energy E of eq 3, which also can be written as

$$E = \int \Psi^* \hat{H} \Psi\, d\tau / \int \Psi^* \Psi\, d\tau \tag{7}$$

By increasing the number of determinants (m_o) as well as basis functions (m), increasingly accurate solutions can be found for E and Ψ.

2.2. Hierarchy of Approximate Wave Function Methods

Only a single determinant D_o is used in the expansion for the wave function Ψ given in eq 4 in the simple Hartree−Fock (HF) theory.[4] The first (minimum basis set) HF calculations carried out on transition metal complexes appeared around 1970.[7] The time required to carry out HF calculations is formally proportional to m.[4] However, the use of efficient algorithms can reduce the time requirement to m^2. For large systems (>1000 atoms), the time required scales linearly[8] with m. The HF method neglects correlation between the movements of electrons of different spins and has only been of limited success in terms of chemical accuracy for transition metal complexes. This is especially true for 3d metals.[9] However, the HF method can be applied routinely to large systems with up to 2000 atoms.

Increasing the number of Slater determinants into the expansion for Ψ given in eq 4 makes it possible to take into account states of different spin. Simpler correlated methods include the second-order Møller−Plesset pertrurbation theory scheme[10] (MP2), the generalized valence bond (GVB) method,[11] and the complete active space scheme (CASSCF).[12] These methods provide reasonable chemical accuracy with time requirements increasing as m^4 with the number of basis functions m. More accurate correlated methods include the coupled-cluster scheme CCSD(T), the multireference approach (MCSCF), as well as the complete active space second-order perturbation theory (CASPT2).[13] Especially, CCSD(T) has been shown to provide high chemical accuracy.[9a] Unfortunately, the CCSD(T) scheme requires large basis sets and scales as m.[6] Thus, CCSD(T) can only serve as a benchmark method for smaller size molecules (20 atoms). The correlation between electrons at close distance (dynamic correlation) is described well by the CCSD(T) scheme. However, there are cases in which the correlation between electrons separated by long distances (nondynamic correlation) is important as well. For these cases,[9b] use must be made of MCSCF and CASPT2 approaches.

2.3. Kohn and Sham Density Functional Theory (DFT)

It has been shown by Kohn and Sham[14] that it is possible by an alternative method to obtain the potential energy E of eq 7 along with other molecular properties without solving for Ψ of eq 3. This alternative method is often referred to as DFT.[15] It is based on a theorem due to Kohn[16] and Hohenberg

according to which the ground state energy E is determined uniquely by the electron density $\rho(\vec{r})$. Unfortunately, the exact functional relation between E and $\rho(\vec{r})$ is not known and the practicality of DFT has largely relied on finding approximate but accurate relations between $\rho(\vec{r})$ and E guided by physical arguments.

For all of the approximate DFT methods[16] developed to date, use is made of n (Kohn−Sham) orbitals to express the electron density of the n-electron system according to

$$\rho(\vec{r}) = \sum_{i=1}^{n} \varphi_i^*(\vec{r})\, \varphi_i(\vec{r}) \tag{8}$$

where the KS orbitals are expressed as a linear combination of basis functions

$$\varphi_i(\vec{r}) = \sum_{k=1}^{k=m} C_{ik}\, \chi_k(\vec{r}) \tag{9}$$

For each DFT scheme, the total energy is written in terms of the density that in turn is expressed in terms of the KS orbitals according to eq 8. The expansion coefficients $\{C_{ik};i = 1,n;k = 1,m\}$ can thus be determined in such a way as to minimize the energy. Thus, the DFT approach requires only the optimization of the orbital coefficients C_{ik} whereas correlated wave function methods in addition to the orbital coefficients also require the optimization of the determinant expansion coefficient $\{c_{ik};\ i = 1,$ large$\}$. This difference makes the DFT approach comparatively faster.

2.4. Jacob's Ladder of Approximate DFT Methods

Kohn[14] suggested as early as 1965 to write E as a functional of $\rho(\vec{r})$ in what became known as the local density approximation (LDA). The LDA method forms the first rung on the ladder of approximate DFT methods as defined by Perdew.[17d] The LDA method affords reasonable geometries but tends to overestimate bond energies.[15d] Becke,[17] Perdew,[18] and others[19] have since 1980 formulated expressions for E in terms of $\rho(\vec{r})$ and its first derivative with respect to $\vec{r}$. These methods are collectively referred to as generalized gradient approximations[17b] (GGA) and considerably improve calculated bond energies as compared to LDA.[9b,15a,d] Well-tested GGA methods are BP86,[17c,18a] BLYP,[19a] PBE,[18b] and RPBE.[19b,c] They form the second rung on the ladder of approximate DFT methods. Most recently, energy expressions containing $\rho(\vec{r})$ as well as its first derivatives and higher order terms have appeared. They are often referred to as Laplacian methods (LAP).[20a−d] The LAP schemes are currently under evaluation for transition metal complexes. They form the third rung on the ladder of approximate DFT schemes and are also referred to as meta-GGA methods. A well-tested recent meta-GGA functional is TPSS.[20m]

An interesting hybrid method suggested by Becke[21] mixes the HF energy expression with that from the BLYP method. This scheme is referred to as B3LYP and is currently the most used approximate DFT method. The B3LYP scheme belongs to the fourth rung on the ladder of approximate DFT methods since its energy depends not only on the density described by the orbitals through eq 8 but also on each individual occupied orbital through the HF exchange. A related hybride functional[20l] (PBE0) mixes PBE with HF. Another promising method from the fourth rung is the self-interaction corrected DFT method (SIC-DFT).[20f,g] At the top of the ladder (quantum mechanical heaven) are the methods with energy expressions that depend on occupied as well as virtual orbitals. The exact wave function method would be such a scheme since the total energy through eqs 4 and 7 can be expressed in terms of all of the occupied and virtual KS orbitals. Other more approximate orbital-dependent schemes are starting to emerge.[20h,i]

The LDA scheme is computationally the most expedient method. However, the time required to study the same system by the GGA and meta-GGA methods increases only by factors of 2 and 3, respectively. The very popular B3LYP scheme requires 2−3 times the resources needed by GGA. For the foreseeable future, most DFT applications are likely to be carried out with B3LYP or (meta-) GGA schemes as these methods strike the right compromise between accuracy and speed. However, there are many cases in which B3LYP and (meta-) GGA fail. These cases include[20j] molecules where bonds are being stretched (bond dissociation and radical recombination) as well as reactions with transitions states where a bond is extended over more than two atoms (S_N2 reactions). For these systems, one will have to develop and apply more accurate orbital-dependent DFT schemes.[20k,l]

3. Exploring the PES

3.1. Energy Gradient and the Accuracy of Optimized Molecular Structures

The development of methods that not only calculate potential energy points but also in an automated way locate local minimum energy points[22] representing stable structures has been of great practical importance. This is done by calculating the forces on all atoms (energy gradients) and stepwise move the atoms in the direction of the forces toward lower energy until the nearest minimum is reached.[4] The ability to locate (optimize) molecular structures is likely the most important function of a modern electronic structure program.

3.1.1. Structures from DFT Methods

Table 1 compares M−C bond distances calculated by different theoretical methods[15a,23b] to experiment for the series $M(CO)_6$ (M = Cr, Mo). We note among the DFT methods that LDA underestimates the M−C bond distances as compared to experiment whereas the two GGA schemes BP86 and RPBE are in much closer agreement with experiment. It is in general observed that LDA M−L bonds are shorter than those obtained by the GGA schemes. Furthermore, for covalent "organometallic bonds" (as in Table 1), the GGA schemes provide better bond distances than

Table 1. Calculated and Experimental M−C and C−O Bond Lengths (Å) for $M(CO)_6$ (M = Cr, Mo)[a]

	M−C	
method	$Cr(CO)_6$	$Mo(CO)_6$
LDA	1.866	2.035
BP86	1.910	2.077
RPBE[a]	1.925	
B3LYP	1.921	2.068
HF	2.00	
MP2	1.883	2.066
CCSD(T)	1.939	
Exp	1.918	2.063

[a] All data are from ref 15a except the RPBE results, which were taken from ref 23b.

Table 2. Statistical Summary[a] of the Errors of Four Density Functionals for Various Molecular Properties

		mean absolute error			
property	mean value	LDA rung 1[t]	PBE[r] rung 2[t]	TPSS[a] rung 3[t]	PBE0[t] rung 4[t]
atomization energy[b]	478[i]	83.8	17.1	6.2	5.1
ionization potential[c]	10.9[k]	0.22	0.22	0.23	0.20
electron affinity[c]	1.4[k]	0.26	0.12	0.14	0.17
bond length[d]	1.56[l]	0.013	0.016	0.014	0.010
harmonic frequency[e]	1430[m]	48.9	42.0	30.4	43.6
H-bond energy[b,g]	13.4[n]	5.8	1.0	0.6	0.7
H-bond length[d,h]	2.06[o]	0.147	0.043	0.021	0.032
H-bond angle[f]	111[p]	4.0	2.6	2.0	1.8

[a] Ref 20m. [b] kcal/mol. [c] eV. [d] Å. [e] cm^{-1}. [f] Deg. [g] Dissociation energy for hydrogen-bonded species. [h] Distance between hydrogen and heteroatom in hydrogen-bonded species. [i] Based on 148 molecules. [j] Based on 86 molecules. [k] Based on 58 molecules. [l] Based on 96 molecules. [m] Based on 82 molecules. [n] Based on 10 complexes. [o] Based on 11 H-bonds. [p] Based on 13 angles. [q] Ref 14. [r] Ref 18a. [s] Ref 20l. [t] Level of DFT method on the ladder of approximate DFT.

LDA. However, for ionic M−L bonds (L = halides[23c] or chalconides[23c,d]), the GGA bonds are too long and the LDA estimates are in some cases closer to the observed values.[23b] Tentative results seem to indicate that SIC-DFT considerably improves M−halide and M−chalconide bond distances.[20g] Also shown in Table 1 are M−C distances from the B3LYP hybrid method. They are seen to compare well with the GGA results. Statistics based on 96 main group molecules indicates that bond distances calculated by the rung 1 LDA method is slightly better than the GGA and meta-GGA results (Table 2). The best results are obtained by the rung 4 functionals such as PBE0 (shown in Table 2) and B3LYP.

3.1.2. Structures from Wave Function Methods

Let us next consider the wave function methods (Table 1). Here, for HF, the Cr−C bond is seen to be much too long whereas it is too short for MP2. It is a general trend that MP2 overcorrects for the HF error in the case of 3d elements. For these elements, CCSD(T) is often required in order to obtain accurate M−L distances. However, for the 4d element molybdenum (and its heavier congener; see later), MP2 is seen to be quite adequate (Table 1). The 3d elements are especially challenging because they have the ns, np, and nd electrons ($n = 3$) in the same region of space. Thus, ligand orbitals are strongly repelled by 3s, 3p as they are seeking stabilizing interactions with the 3d orbitals. The result is relatively long M−L distances and poor overlaps between the 3d set and the ligand orbitals. This in turn results in modest highest occupied molecular orbital−lowest unoccupied molecular orbital gaps and a considerable amount of nondynamic correlation.[23g] For the heavier congeners ($n = 4, 5$), ns and np are well-separated from nd.

Table 3. Calculated and Experimental W−C Bond Distances (Å) and First W−CO Bond Dissociation Energies (kcal/mol), FBDEs, for $W(CO)_6$[a]

	$W(CO)_6$	
method	W−C	FBDE
BP86[b]	2.116	38.8
BP86+R[c]	2.049	43.7
B3LYP[c]	2.078	44.8
HF		37.7
MP2[c]	2.060	54.9
CCSD(T)[c]		48.0
Exp	2.058	46.0 ± 2

[a] Data from ref 9c. [b] Calculations without relativistic effects. [c] Calculations with relativistic effects included.

3.2. Relative Energies between Reactants and Products

Another test of the quality of the theoretical PES is the calculated relative energies between reactants and products. Table 3 displays the energies required to dissociate the first CO ligand from $M(CO)_6$ (M = Cr, Mo). We note among the DFT schemes that LDA overestimates the bond energy, and this is a general result for all M−L dissociations. For the GGA schemes, Table 3 and work by Rösch et al.[23b] seem to indicate that the RPBE is the most accurate method. However, all of the GGA schemes seem to afford M−L dissociation energies with an accuracy of ±5 kcal/mol. The data from Table 3 would indicate that B3LYP has an even smaller error margin. The performances of both BP86[9a,15a,24] and B3LYP[9a,15a,25] for transition metal complexes have been reviewed.

For main group elements, the energetics clearly improves in going from rung 1 to rung 4 of the DFT ladder; see Table 2. Thus, GGA is a substantial improvement over LDA for atomization energies whereas the meta-GGA scheme presents a further enhancement over GGA with the rung 4 scheme PBE0 affording the most accurate estimates. A similar trend is found for the weak hydrogen bonding, with the exception that no further improvement is obtained in going from rung 3 to rung 4 (Table 2).

Among the wave function methods, the HF scheme finds the first CO dissociation energy to be too small for both metals with the larger error for chromium. The MP2 approach overcompensates for this by finding too strong an M−CO bond, especially in the case of chromium. Only CCSD(T) is able to afford a quantitative fit with experiment. It is in general found that M−L bond energies containing 3d elements require highly correlated methods [CCSD(T)] for a quantitative treatment. In many cases, such a treatment is also recommended for 4d elements and their heavier congeners.[23f−h] It is possible to analyze the M−L bond strength in terms of donor/acceptor

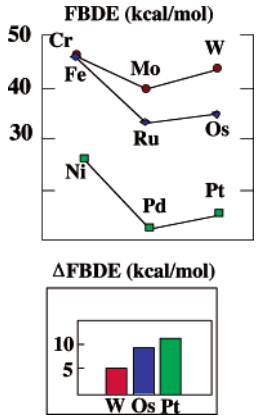

Figure 2. FBDE: Calculated first M−CO bond dissociation energies for $M(CO)_4$ (M = Ni, Pd, Pt), $M(CO)_5$ (M = Fe, Ru, Os), and $M(CO)_6$ (M = Cr, Mo, W) with relativistic effects included. ΔFBDE: Relativistic contributions to FBDE for the three 5d elements.

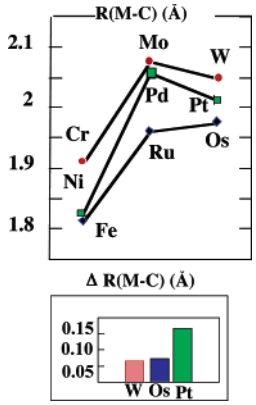

Figure 3. R(M−C): Calculated M−CO bond distances for $M(CO)_4$ (M = Ni, Pd, Pt), $M(CO)_5$ (M = Fe, Ru, Os), and $M(CO)_6$ (M = Cr, Mo, W) with relativistic effects included. ΔR(M−C): relativistic contraction of the M−C bond.

interactions and $\sigma/\pi/\delta$ bonding,[9c,d] as we shall discuss shortly.

3.3. Importance of Relativistic Corrections for Structures and Energies

Valence electrons in atoms and molecules have a finite (albeit small) probability of being close to the nuclei, and they can as a consequence acquire high instantaneous velocities. In fact, the velocities for valence electrons can approach that of light as they pass in close proximity to heavier nuclei with $Z > 72$. It is for this reason not too surprising that relativistic effects[26] become of importance for chemical properties of compounds containing 5d block elements in the third transition series.[27] The two main relativistic effects are the mass−velocity term, which takes into account that the mass of the electron is increased at high velocities, as well as the spin−orbit coupling term. These effects can be included without considerably increasing the computational cost[27b] thanks to the development of a number of relativistic extensions to existing DFT and wave function methods.[27b]

Table 3 displays calculated and observed W−C bond distances and first W−CO dissociation energies. All entries, except BP86, are based on calculations with relativistic corrections included. We note that the nonrelativistic BP86 calculations afford a W−C bond that is too long and too weak as compared to experiment. By adding relativistic effects (BP86+QR), the bond is contracted by 0.066 Å and enhanced in strength by 4.9 kcal/mol. Both corrections considerably improve the agreement with experiment. The other relativistic calculations based on B3LYP and CCSD(T) afford estimates in similar good agreement with experiment. However, HF and MP2 are again seen to respectively underestimate and overestimate the W−CO bond energy.

The relativistic bond contraction and stabilization for 5d elements are general phenomenons. They are responsible for the experimental observation that M−L bonds for 4d elements often are slightly longer and somewhat more labile than the corresponding bonds involving 5d element.[27b,28] Figure 2 displays calculated[27b] first M−CO bond dissociation energies for $M(CO)_4$ (M = Ni, Pd, Pt), $M(CO)_5$ (M = Fe, Ru, Os), and $M(CO)_6$ (M = Cr, Mo, W) with relativistic effects included. We see for all three series of metal carbonyls that the weakest M−CO bond is formed by the 4d elements Pd, Ru, and Mo. Also shown at the bottom of Figure 2 are the relativistic bond stabilizations for the 5d elements. The corresponding stabilizations for 4d elements amount to at the most 1 kcal/mol whereas they are negligible for 3d elements. It follows that the M−CO of the 5d elements would be the weakest within a triad without the relativistic stabilization, which can amount to as much as 10 kcal/mol.

Figure 3 illustrates the M−CO bond contraction[27b] for the same series of carbonyls. For $M(CO)_6$ (M = Cr, Mo, W) and $M(CO)_4$ (M = Ni, Pd, Pt), the longest bond is for the 4d elements M = Mo, Pd. Without the relativistic bond contraction, the longest M−CO bond would be with the 5d element for all three series. It follows further that the relativistic bond contraction is as large as 0.15 Å for M = Pt (bottom of Figure 3). The origin of the relativistic bond contraction and stabilization can ultimately be traced back to the mass increase of valence electrons (mostly in s orbitals) moving near the nuclei. This mass increase will reduce the kinetic energy, which in turn allows the bonds to contract and stabilize.[26−29] The relativistic bond contraction and stabilization are especially important for compounds containing gold and mercury.[26,29a] However, it is also noticeable for actinides.[30] Relativistic bond expansions are comparatively uncommon and might come along with a bond stabilization (e.g., PbO) or destabilization (e.g., AuF and AuCl).

3.4. Analysis of Bond Strengths

The factors that shape the strength of a chemical bond can be analyzed in terms of well-established chemical concepts by making use of energy decomposition schemes. In these schemes, the M−L bond strength is analyzed[9a−d] in terms of donor/acceptor interactions and $\sigma/\pi/\delta$ bonding; see Figure 4. Some of the more common methods are the energy decomposition analysis scheme by Kitaura and Morakuma,[9e,f] the extended transition state (ETS) method by Zie-

Table 4. ETS Decomposition of FBDE (kcal/mol) for $(CH_3)_3P = E$,[a] and $Cp_2Ti = E$[a,f] with E = O, S, Se, Te

bond	DE_o[c]	DE_s[d]	DE_p[e]	FBDE[b]
PdO	255.2	−347.2	−38.0	130.0
PdS	86.0	−141.2	−25.3	80.5
PdSe	67.6	−109.7	−21.5	63.6
PdTe	47.3	−71.9	−19.4	44.0
TidO	326.2	−430.7	−39.4	143.9
TidS	207.9	−267.9	−33.5	93.5
TidSe	180.2	−232.3	−28.5	80.6
TidTe	161.0	−192.6	−30.1	61.7

[a] From ref 23i. [b] FBDE = $-\Delta E_o - \Delta E_\sigma - \Delta E_\pi$. [c] Steric interaction energy; see refs 23d,i as well as Scheme 1. [d] Interaction energy due to σ-bond formation. [e] Interaction energy due to π-bond formation. [f] From ref 23d.

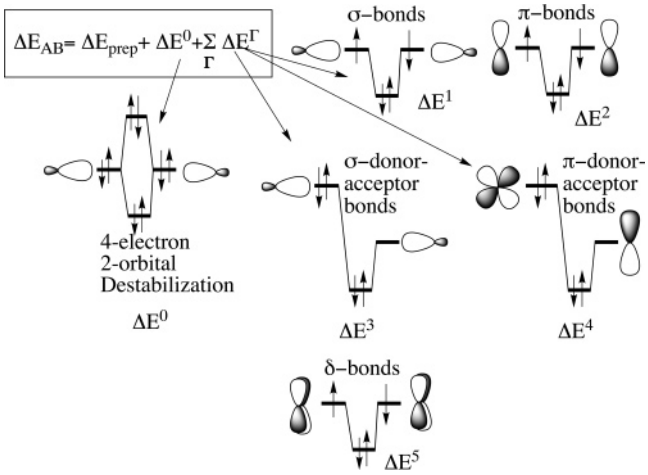

Figure 4. Energy decomposition in terms of donor/acceptor interactions and $\sigma/\pi/\delta$ bonding according to ref 9g.

gler and Rauk,[9g,h] and the constrained space orbital variation method by Bagus, Hermann, and Bauschchlicher.[9i]

The top of Table 4 provides data from a decomposition analysis[23i] of the multiple P=E bond in $(CH_3)_3$-P−E (E = O, S, Se, Te) as an example of multiple bonds between main group elements and chalcogenides. The $(CH_3)_3P$=E bond is established by electron donation from a PR_3 σ-orbital to an empty p_σ orbital on the chalcogenide, see Figure 4, as well as π-back-donations from p_π of E, Figure 4, to a degenerate pair of low-lying PC σ^* orbitals on PMe_3. The P−E bond strength is seen to decrease from oxygen to tellurium. This is primarily due to a corresponding decrease in the contribution, ΔE_σ, from the σ-bond interaction as the energy gap between the two σ-orbitals diminishes. The π-back-donation ΔE_π is not negligible for any of the systems. It attains further a proportionally larger importance toward the end of the family as it decreases much more slowly than ΔE_σ. It might be surprising that ΔE_π is largest for the more electronegative element oxygen. This is a synergistic effect. As charge is built up on oxygen in the σ-donation, there is a strong need to relieve the excess density by π-back-donation.

Data[23d] from a similar study of the Ti=E multiple bond in Cp_2Ti=E (E = O, S, Se, Te) are provided at the bottom of Table 4 as an example of multiple bonds between a metal and a chalcogenide. Here, the σ-bond is established as a donation of density from the occupied d_σ orbital on Cp_2Ti to the empty p_σ orbital on E. On the other hand, the π-bond is due to back-donation of charge from one occupied p_π orbital on E to the empty d_π orbital on Cp_2Ti. It is clear from Table 4 that the Ti=E bond decreases in strength with decreasing electronegativity of E and that this trend is determined by the σ-donation. Simply, the transfer of charge from the metal is most favorable for oxygen with the most stable p_σ orbital. The π-back-donation ΔE_π is less important in absolute terms and decreases from oxygen to tellurium. However, in relative terms, the importance of π-back-donation increases from E= O to E=Te.

Table 5. ETS Decomposition[a] of FBDE (kcal/mol) for $Pt(CO)_4$, $Os(CO)_5$, and $W(CO)_6$ at the Nonrelativistic-B86 (NR) and Relativistic-B86 (R) Levels

complex	method	DE_o[c]	DE_s[d]	DE_p[e]	DE_{prep}[f]	FBDE[b]
$Pt(CO)_4$	NR	51.6	−25.5	−31.0	2.8	2.1
	R	47.7	−30.7	−35.6	2.9	15.7
$Os(CO)_5$	NR	69.5	−54.5	−42.5	4.0	23.5
	R	65.3	−37.3	−67.2	4.5	34.7
$W(CO)_6$	NR	39.5	−29.2	−44.2	0.3	34.2
	R	35.0	−19.6	−60.1	1.0	43.7

[a] From ref 27b. [b] FBDE = $-\Delta E_o - \Delta E_\sigma - \Delta E_\pi - \Delta E_{prep}$. [c] Steric interaction energy; see ref 27b and Scheme 1. [d] Interaction energy due to ligand-to-metal σ-donation. [e] Interaction energy due to metal-to-ligand π-donation. [f] Preparation energy. The energy required to go from the structures of free CO and $M(CO)_{n-1}$ to the structures that the two fragments have in the combined complex $M(CO)_n$.

The decomposition scheme can also be used to analyze how relativistic effects influence the M−CO bond strengths as it was discussed previously in connection with Figures 2 and 3. Table 5 displays an ETS decomposition of the FBDEs for the three third row metal carbonyls according to the process $M(CO)_n \rightarrow M(CO)_{n-1} + CO$−FBDE, at the nonrelativistic BP86 (NR) and relativistic (R) BP86 levels of theory. For $Os(CO)_5$, consideration was only given to the case where an equatorial CO ligand is removed. The bonding in these species is represented by donation of density from the σ_{C-O} orbital of the leaving CO ligand to empty orbitals on the $M(CO)_{n-1}$ fragment (ΔE_σ) as well as back-donation from the occupied d_π orbitals on the $M(CO)_{n-1}$ fragment to empty π_{C-O}^* orbitals on the leaving CO ligand (ΔE_π). As can be seen from Table 5, relativistic effects increase the contribution to the bond energy from the d_π to π_{C-O}^* back-donation interaction, ΔE_π. This trend is understandable in considering the general relativistic destabilization[27b] of 5d orbitals for third row atoms. The higher energy of d_π will reduce the $d\pi-\pi_{C-O}^*$ gap and thus enhance the back-donation interaction. The effect is smallest in $Pt(CO)_4$ where the d levels are lowest in energy as compared to π_{C-O}^*. Because the back-donation interaction is the dominant stabilizing contribution to the M−CO bond energies, relativity increases in all cases the FBDEs. The contribution from the σ_{C-O} to metal donation interaction (ΔE_σ) is reduced by relativity in the cases of M=W and Os due to the destabilization of the 5d orbitals, which makes $5d_\sigma$ a poorer acceptor orbital. In the case of

$Pt(CO)_4$, the donation is to a metal-based orbital with an appreciable 6s contribution, and ΔE_σ is increased by relativity due to the relativistic stabilization[27b] of 6s.

3.5. Potential Energy Curvatures and Vibrational Frequencies

The PES of a molecule of N atoms can be expanded in a Taylor series around the nuclear configuration $Q^o\{ X_i^o, i = 1,N\}$ to second order in terms of the Cartesian nuclear displacements $\Delta Q\{ \Delta X_i = X_i - X_i^o, i = 1,3N\}$ as[31a]

$$U(Q^o + \Delta Q) = U(Q^o) + \sum_i^{3N} \vec{g}_i^{\,o}\, \Delta X_i + \frac{1}{2}\sum_i^{3N}\sum_j^{3N} H_{ij}^{\,o}\, \Delta X_i\, \Delta X_j + \text{higher order terms} \quad (10)$$

where

$$\vec{g}_i^{\,o} = \left(\frac{\delta U}{\delta X_i}\right)_o \quad (11)$$

is the potential energy gradient around Q^o and

$$H_{ij}^{\,o} = \left(\frac{\delta^2 U}{\delta X_i\, \delta X_j}\right)_o \quad (12)$$

is the potential energy Hessian.

For equilibrium structures, the potential energy gradient is zero and the potential energy is thus quadratic (harmonic) with respect to (small) nuclear displacements. In this case, the nuclei will vibrate as harmonic oscillators with fundamental frequencies (ν_i) given by $\nu_i = 1/2\pi\sqrt{\lambda_i}$, where λ_i is an eigenvalue to the eigenfunction equation[31b]

$$F\, C_i = \lambda_i\, C_i \quad (13)$$

and F is the mass-weighted potential energy Hessian with elements $F_{ij} = M_i^{-1/2} H_{ij} M_j^{-1/2}$, where M_k is the nuclear mass for the atom with which the kth Cartesian coordinate is associated. The displacement $\vec{R}_i$ (normal mode) associated with ν_i can finally be expressed in terms of the eigenvectors as

$$\vec{R}_i = \sum_k C_{ki}\, M_k^{\,1/2}\, \Delta X_k\, \vec{e}_k \quad (14)$$

We note that eq 13 will have six solutions with zero eigenvalues corresponding to the three rigid translations and rotations of the molecule.

The ability to calculate the potential energy gradients of eq 11 analytically[22] has been of great practical importance for the efficient optimization of molecular structures. A further important step forward in the characterization of the PES was taken by the efficient analytical evaluation of the energy Hessian[31c,d] in eq 12. The Hessian makes it further possible to characterize stationary points where $\vec{g}_i^{\,o} = 0$ in terms of energy minima where all eigenvalues of eq 13 are zero or positive and the TS in which one eigenvalue is negative. The eigenvalues $\{\lambda_i; i = 1,3N - 6\}$ make it further possible to calculate the fundamental harmonic frequencies (ν_i), which can be observed experimentally.

It follows from Table 2 that the mean absolute errors in frequencies calculated by rung 1 (LDA), rung 2 (PBE), rung 3 (TPSS), and rung 4 (PBE0) DFT methods are, respectively, 48.9, 42.0, 30.4, and 43.6 cm^{-1} for a large sample of main group molecules where the average frequency was 1400 cm^{-1}. The corresponding value[31e] for B3LYP (rung 4) is 34 cm^{-1}. The errors for wave function methods[31e] are 56 (HF), 60 (MP2), and 37 (QCISD) cm^{-1}, respectively. Thus, only the highest level of wave function methods (QCISD) affords the same level of accuracy as standard DFT schemes such as PBE (rung 2) or B3LYP (rung 4).

3.6. Reaction Paths and TSs

The TS in Figure 1 represents the lowest energy point on the ridge that separates the valley of the reactants from the valley of the products. It is characterized by having zero forces ($\vec{g}_i^{\,o}$ of eq 11) on all atoms as well as one and only one normal mode ($\vec{R}_i$ of eq 14) with an imaginary frequency. This normal mode defines the reaction coordinate (RC) of Figure 1 in the vicinity of the TS. The remaining part of the RC in Figure 1 is obtained by performing a steepest descent (in terms of energy) from the TS to the reactants and the products, respectively. This pass is most often referred to as the MEP since its direction locally always is toward lowest energy. The RC for the process is defined as all of the conformations of the chemical system corresponding to points on the MEP, and the energy profile is the corresponding energy points on the PES.[31h]

3.6.1. Optimizing TSs

Locating TSs requires an element of chemical insight and has not yet been fully optimized from the specification of the reactants and the products. Strategies involve (i) finding the ridge separating reactants and products and searching for the minimum point on the ridge;[32a] (ii) converging an initial path from reactants to products towards the MEP by iteratively finding new paths in which forces perpendicular to the RC are minimized;[32b] (iii) searching along a preconceived RC;[32c] and (iv) following a normal mode with an imaginary frequency toward higher energies.[32d,e] Ultimately, the determined structure must have zero forces on all atoms and only one imaginary frequency to qualify as a TS. Furthermore, the corresponding reactants and products can be found by a steepest descent to the nearest minimum.

3.6.2. Tracing the MEP

The movement of the N nuclei during a chemical reaction can be described in classical mechanics, by the following equations of motion:

$$d(m_\alpha \dot{X}_\alpha) = -\frac{\partial U}{\partial X_\alpha} dt$$

$$d(m_\alpha \dot{Y}_\alpha) = -\frac{\partial U}{\partial Y_\alpha} dt$$

$$d(m_\alpha \dot{Z}_\alpha) = -\frac{\partial U}{\partial Z_\alpha} dt \quad (15)$$

where $\alpha = 1, 2, ..., N$, m_α is the mass, $(X_\alpha,Y_\alpha,Z_\alpha)$ are the Cartesian coordinates of the αth atom, $(\dot{X}_\alpha,\dot{Y}_\alpha,\dot{Z}_\alpha)$ are the corresponding time derivatives, and U is the potential energy of the reaction system. Equation 15 completely defines the path $\xi(t) = [X_1(t), Y_1(t), Z_1(t), ..., X_N(t), Y_N(t), Z_N(t)]$ of the nuclei during the reaction for a given set of initial velocities at time $t = 0$. Fukui defined the MEP from the conditions that the nuclei move with an infinitesimal velocity at any given point. By using this assumption and integrating eq 15 over t, it follows that

$$\frac{m_\alpha dX_\alpha}{\partial U/\partial X_\alpha} = \frac{m_\alpha dY_\alpha}{\partial U/\partial Y_\alpha} = \frac{m_\alpha dZ_\alpha}{\partial U/\partial Z_\alpha} = -t\, dt \quad (16)$$

where $\alpha = 1, 2, ..., N$. Further introducing the mass-weighted coordinate: $x_{3\alpha-2} = m_\alpha^{1/2} X_\alpha$, $x_{3\alpha-1} = m_\alpha^{1/2} Y_\alpha$, $x_{3\alpha} = m_\alpha^{1/2} Z_\alpha$, $\alpha = 1, 2, ..., N$, and the parameter $d\tau = t\, dt$ (>0) reduces eq 16 to the MEP equation

$$\frac{dx_i}{\partial U/\partial x_i} = -d\tau \quad (17)$$

where $i = 1, 2, ..., 3N$, or in vector form

$$d\mathbf{x} = -\vec{g}_x\, dt \quad (18)$$

where $\mathbf{x} = (x_1, x_2, ..., x_{3N})^T$ and $\vec{g}_x = \nabla_x U = (\partial U/\partial x_1, \partial U/\partial x_2, ..., \partial U/\partial x_{3N})^T$. It is customary to refer to $\mathbf{x}$ of eq 4 as the intrinsic reaction path[34] or the MEP.[31h]

Equation 18 underlines that the displacement on the MEP is in the steepest direction along $-\vec{g}_x$. Thus, the change in coordinates along the MEP is identical to the steepest decent path in the mass-weighted Cartesian coordinate system. The MEP is often written as $\mathbf{x}(s)$ where s is the length of MEP at $\mathbf{x}(s)$ with $s = 0$ corresponding to the TS. Using that $ds^2 = d\mathbf{x} \cdot d\mathbf{x}$ gives according to eq 4 $ds = |\vec{g}_x|\, d\tau$. Thus, eq 18 can be written in terms of s as

$$\frac{d\mathbf{x}}{ds} = -\frac{\vec{g}_x}{|\vec{g}_x|} \quad (19)$$

which is the standard form for Fukui's IRC equation in mass-weighted Cartesian coordinates.

Fukui[33c] et al. have shown that MEP is a quasi-geodesic curve in Riemannian space and thus the shortest path connecting reactant to product via the TS. Igawa[33d] et al. proved that the MEP corresponds to the least motion path, which is the most favorable reaction pathway according to the principle of least motion.

In practice, the solution to the MEP eq 19 can be obtained by a Taylor expansion of $\mathbf{x}(s)$ in terms of s starting from the TS ($s = 0$):

$$\mathbf{x}(s) = \mathbf{x}(s_0) + \Delta s \left.\frac{d\mathbf{x}}{ds}\right|_{s=s_0} + \frac{(\Delta s)^2}{2!} \left.\frac{d^2\mathbf{x}}{ds^2}\right|_{s=s_0} + ... + \frac{(\Delta s)^n}{n!} \left.\frac{d^n\mathbf{x}}{ds^n}\right|_{s=s_0} + ... \quad (20)$$

where $\Delta s = s - s_0$. Equation 20 relates two points $\mathbf{x}_{k+1}(s_0 + \Delta s)$ and $\mathbf{x}_k(s_0)$ on the MEP. For sufficiently small values of Δs, only terms up to $n = 1$ are required, and we get with the aid of eq 19

$$\mathbf{x}_{k+1} = \mathbf{x}_k - \Delta s \frac{\vec{g}_k}{||\vec{g}_k||} \quad (21)$$

Hratchian and Schlegel[33e] have recently developed a method in which larger steps (Δs) can be used in the integration along the MEP by taking into account terms up to $n = 2$ in eq 20.

Constructing the MEP can be a useful tool in a more detailed study of a chemical reaction.[33] As an illustration, consider the O−H activation of methanol by $CrCl_2O_2$ to produce $CrCl_2(O)OH)(OCH_3)$ (Scheme 1). The process has a four center TS (TS1 of Scheme 1). Figure 5 displays the change in the internal coordinates of the reaction system from reactants ($s = -10$) over the TS ($s = 0.0$) to the products ($s = 10.0$), where s is the length of the MEP from the TS (counted negative in the direction of the reactant). We note that the OH methanol bond (f of TS1 in Scheme 1) is broken just before the TS whereas the new OH bond (g of TS1 in Scheme 1) is formed right after the TS. Note also a decrease in the Cr−H bond at $S = 0$, as the metal assists the passage of hydrogen from one oxygen to another.

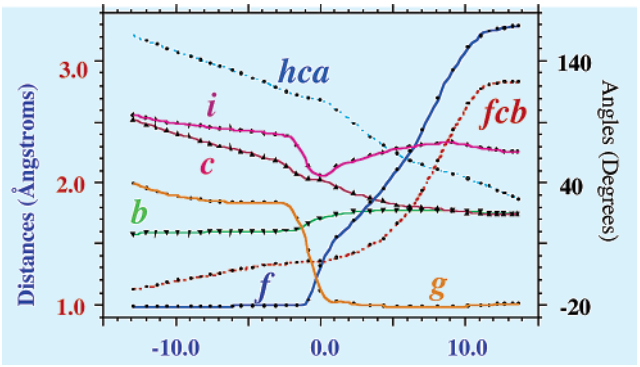

Figure 5. Change in internal coordinates along the MEP for the reaction $CrCl_2O_2 \rightarrow CrCl_2(O)OH)(OCH_3)$. Reactants ($s = -10$), TS ($s = 0.0$), and products ($s = 10.0$).

Scheme 1. Schematic Presentation of the Structural Changes in the Reaction $CrCl_2O_2 \rightarrow CrCl_2(O)OH)(OCH_3)$

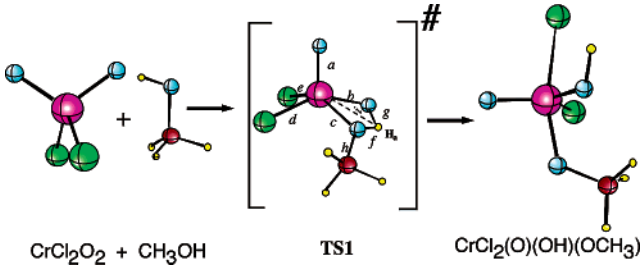

4. Influence of Environmental Effects on PES

4.1. Representing Steric Bulk

The computational modeling of inorganic reactions necessitates as we have seen a high level quantum mechanical treatment because lower level methods cannot accurately treat the bond breaking and forming that occurs during these processes. However, a high level quantum mechanical study often involves a stripped down model system that only vaguely resembles the true system. An example of this is depicted in Figure 6 where the "real" catalyst system that is being modeled is shown in (a), while a likely model of it used for a quantum mechanical calculation is shown in (b). Thus, if large ligands are involved, they are most often neglected in high level calculations with the hope that they do not substantially influence the nature of the reaction mechanisms. Unfortunately, the surrounding ligand system, protein matrix, or solvent can often play a critical mechanistic role. One dramatic example in organometallic catalysis is that of the recently developed Ni(II) Brookhart polymerization catalyst,[34] **1** (Figure 6). Without an extended ligand system, the catalyst acts only as a dimerization catalyst. However, by attaching an extended and sterically demanding ligand system, Brookhart and co-workers were able to transform the poor polymerization catalyst into a commercially viable one. Therefore, quantum mechanical models, which do not treat the extended ligand structure or solvent environment, may yield results that are inconclusive, suspect, or possibly erroneous. Even with the rapid development of computer technology and modern linear scaling methods,[8,35] the full quantum mechanical treatment of these extended systems is not expected to be practical soon.

One reasonable approach to escape this problem is the combined quantum mechanics and molecular mechanics (QM/MM) method.[36] In this hybrid method, part of the molecular PES, such as the active site region, is determined by a quantum mechanical calculation while the remainder of the molecular potential is determined using a much faster molecular mechanics force field calculation. Such a partitioning is illustrated in Figure 6c. The promise of the QM/MM method is that it allows for simulations of bond breakage and formation at the active site, while still allowing for the role of the extended system to be modeled in an efficient and computationally tractable manner. The key feature of the QM/MM method is that the QM calculation is performed on a truncated "QM model" (Figure 6b) of the active site, where the large ligands have been removed and replaced with capping atoms (in the current case hydrogens). Then, a molecular mechanics calculation is performed on the remainder of the system and the effects of the attached ligands are incorporated to form the potential surface of the whole system where the QM and MM regions interact with one another via steric and electrostatic potentials.

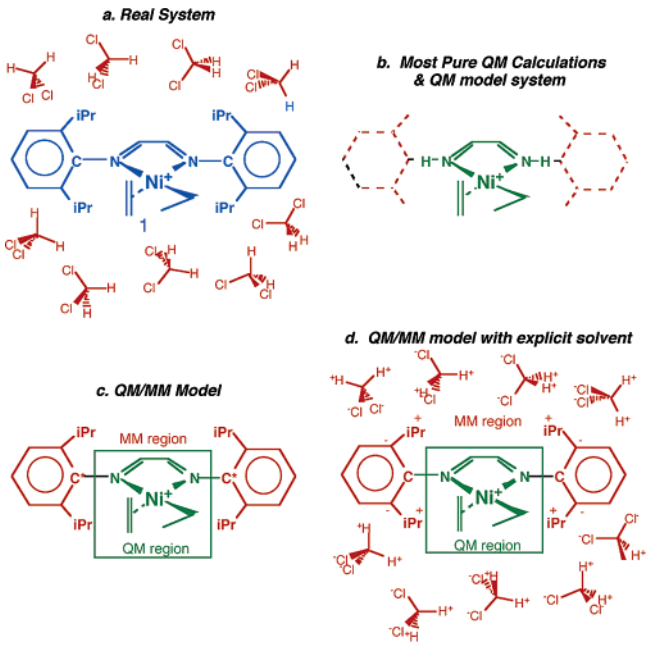

Figure 6. Brookhart Ni(II) bisimine catalyst.

The combined QM/MM methodology dates back to work by Warshel and Levitt[36a] in 1976, but it was not until 1986 that a practical QM/MM prescription was developed by Singh and Kollman.[36a] Despite its history, QM/MM methods have only recently received serious attention as a practical modeling tool to examine extended systems too large for pure QM methods. The QM/MM modeling of proteins has also been successful despite the impressive challenges that these complicated macromolecules impose. An area, which has only begun to be explored with hybrid QM/MM potentials, is transition metal-containing catalytic systems, such as metalloenzymes[37a] and organometallic complexes.[37b] It is also possible to make hybrids between different levels of purely quantum mechanical methods.[37c] In all cases, care must be given to how one divides up the chemical system as well as to how one stitches the different regions together afterward.[37d] It is worth to mention that a pure molecular mechanics (MM) approach has been used successfully in many cases, especially those not involving bond breaking or bond formation.[37e] We shall now in the next section discuss how one can incorporate the influence of the solvents shown in Figure 6d.

4.2. Solvation Effects

The presence or absence of solvent in a chemical system can lead to completely different chemical behavior and reactivity. For this reason, the incorporation of solvent effects into quantum mechanical PESs has been and still is an active area of theoretical chemistry. Methods for introducing solvent effects in quantum chemical calculations can be broadly divided into two categories[38]—(i) continuum models[39−41a] and (ii) explicit solvent models.[41b] With continuum models, the solvent molecules are not treated explicitly but rather they are expressed as a homogeneous medium characterized by a bulk dielectric constant. This is shown pictorially in Figure 7a. The effect of the solvent is modeled by a buildup of charge[42] on the continuum surface such that there is a polarization of the QM wave function within the

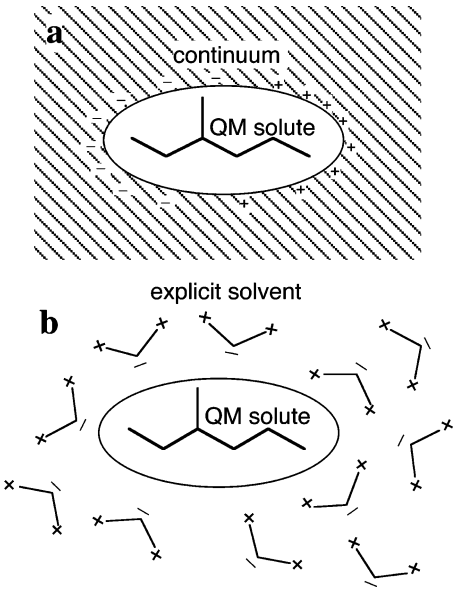

Figure 7. Modeling solvation with a (a) continuum model and (b) explicit solvent molecules.

solute cavity. The amount of charge buildup and subsequently the polarization of the wave function are a function of the dielectric constant of the solvent. Continuum models have been quite successful in capturing the general aspects of solvation and in many cases can be used for quantitative predictions. Because the solvent molecules are not treated explicitly, continuum models are relatively efficient. On the other hand, the lack of an explicit treatment has the disadvantage that continuum models do not provide any specific information concerning the intermolecular interactions.[43] The two most popular continuum methods are the polarizable continuum method[40] and the conductor-like screening model (COSMO).[39]

The other broad approach to introducing solvent effects into the quantum mechanical potential surface is to treat the solvent molecules explicitly. With standard electronic structure calculations, this is achieved by surrounding the solute molecule with solvent molecules—all of which are treated quantum mechanically. For ab initio level calculations, generally only a few solvent molecules can be included. Although the interactions between the solvent molecules and the solute molecule are treated rigorously, a few solvent molecules do not simulate the bulk solvent. Therefore, even qualitative conclusions can be dubious in nature. Recently, the Car−Parrinello (CP)[44] molecular dynamics (MD) method (see later) has allowed for simulations of bulk liquid to be carried out at the density functional level.[45,46] Although the approach is promising, it is still impractical for anything but the smallest solute and solvent molecules (e.g., water in water and methanol in water). The combined QM/MM approach seems well-suited for performing explicit solvation simulations. A natural partition exists such that the solute is treated with QM, while the explicit solvent molecules are handled by a much more efficient MM force field. Pioneering the approach, Gao and co-workers[47] have demonstrated that the QM/MM method can be used to predict solvent polarization effects at the quantitative level for such properties as reaction barriers, equilibrium constants, and solvation free energies. Explicit solvation will be under development as an active research area for the next 10 years.[48] A method beyond the continuum scheme that provides a realistic description of the molecular liquids of various complexities is the reference interaction site model (RISM)[41b] integral equation theory. This method considers the solute in a mean field due to the solvent molecules averaged over all orientations. The RISM scheme is still expensive and under development. Meanwhile, continuum models are likely to be used extensively in the day-to-day modeling of chemical reactions.

Table 6. Experimental and Theoretical Dipole-Allowed Excitation Energies[a] in $Ni(CO)_4$

	band			
method	I	II	III	IV
CASSCF	7.3	7.5	7.6	7.7
CASPT2	4.3	5.2	5.6	6.3
SAC-CI	4.8	5.5	5.7	5.8
TDDFT	4.7	4.8	5.4	5.8
exp.	4.5	5.4	5.5	6.0

[a] All data (in eV) from ref 49.

5. Excited States

We have up to now only discussed the PES for the ground state. However, above at higher energies are the PESs of the excited states. These surfaces have been probed experimentally by spectroscopic and photochemical methods.[49] For transition metal complexes, crystal- and ligand-field theory have been used extensively to rationalize the large body of experimental data.

The first ab initio wave function calculations[7a] on transition metal excitation energies were met with very little success as they included no (HF) or limited electron correlation. This is perhaps not so surprising since the degree of electron correlation can differ between two excited states or between the ground state and an excited state. It is now clear that highly correlated methods are required for a proper description of excited states. This is underlined in Table 6 where experimental[50] excitation energies for $Ni(CO)_4$ are compared to those obtained by CASSCF,[12] CASPT2,[13] and the symmetry-adapted cluster configuration interaction (SAC-CI)[51] scheme. It is noted that the CASSCF method with a fair degree of correlation fails to represent the absolute value of the excitation energies as well as the spacing between them. However, the very expensive CASPT2 and SAC-CI schemes both reproduce the observed spectrum well.

DFT is in its original formulation a ground state theory.[16] However, it has been common practice to apply it to excited states by promoting electrons to KS orbitals (eq 8) of higher energy[52] than those occupied in the ground state. This procedure has been termed DFT-ΔSCF, and it has been used extensively. In fact, the first DFT calculations in chemistry successfully made use of schemes[53] similar to DFT-ΔSCF in calculations on excitation energies for

Table 7. Experimental and Theoretical Dipole-Allowed Excitation Energies[a] in MnO_4^-

	band			
method	I	II	III	IV
SAC-CI	2.57	3.58	3.72	5.82
DFT-DSCF	2.57	3.42	3.76	5.99
TDDFT	2.63	3.60	4.52	5.46
exp.	2.27	3.47	3.99	5.45

[a] All data (in eV) from ref 49.

transition metal complexes. Quite recently, a rigorous theory has been developed for the calculation of excitation energies within the framework of DFT.[54] The theory is based on time-dependent perturbation theory (TDDFT),[54d] and it has even been extended to the optimization of excited state structures.[54e] Table 6 illustrates that the excitation energies calculated by TDDFT for $Ni(CO)_4$ are of the same quality as those obtained by the much more expensive CASPT2 and SAC-CI wave function methods

The electronic spectrum of the permanganate ion MnO_4^- has served[50,55] as a testing ground for new computational methods, and only a few have passed the test due to the complicated electronic structure[23g] of this seemingly simple system. It is clear[50] from Table 7 that DFT-ΔSCF, TDDFT, and SAC-CI all reproduce the electronic spectra with reasonable accuracy, although the assignment of the second and third bands differs among the methods (not shown[50]). Unfortunately, the CASPT2 scheme is too expensive for this molecule.[50c]

It is likely that TDDFT (and to some degree DFT-ΔSCF) increasingly will be used to explore the excited state PESs of inorganic molecules, and many applications on large molecules[56] have already appeared. In this respect, the less expensive DFT-ΔSCF scheme can be used to map out the variation of the energy with geometry whereas TDDFT can provide more accurate energy information at particular geometries. The role of the more expensive CASPT2 and SAC-CI wave function methods will be to serve as benchmark methods for smaller molecules.

6. Spectroscopic Methods

Spectroscopic methods are often used to monitor a chemical reaction or identify intermediate species. It is therefore natural to briefly discuss here how theoretical methods are able to calculate spectroscopic parameters from first principle. We have already previously discussed some aspects of vibrational and electronic spectroscopy.

6.1. NMR Chemical Shift[57]

Classically, the interaction of a nuclear magnetic moment $\vec{\mu}_A$ with an external magnetic field $\vec{B}$ is given by

$$E = -\vec{\mu}_A \cdot \vec{B} \tag{22}$$

For nuclei in atoms or molecules, however, it is experimentally observed that the external field is shielded by the electrons and the nucleus interacts with an effective field such that

$$E = -\vec{\mu}_A \cdot (1 - \vec{\sigma})\vec{B} \tag{23}$$

Here, $\vec{\sigma}$ is the nuclear shielding tensor for a nucleus A in a given environment. Quantum mechanically,[58] $\vec{\sigma}$ is given by the second derivative of the total energy (excluding the term in eq 22) with respect to $\vec{\mu}_A$ and $\vec{B}$ as

$$\vec{\sigma}_A = \left(\frac{\delta^2 E}{\delta\vec{B}\,\delta\vec{\mu}_A}\right)_{\vec{B}=0;\vec{\mu}_A} \tag{24}$$

in formal agreement with eq 23. $\vec{\sigma}$ is dimensionless and is usually reported in units of 10^{-6} (part per million = ppm). Its rotational average σ is the isotropic shielding constant. Experimental data from NMR spectroscopy usually refer to the chemical shift of a nucleus, i.e., the change of σ with respect to a reference nucleus in a reference compound. The chemical shift δ in terms of the shielding constants of the two nuclei is given by

$$\delta = \sigma_{\text{reference}} - \sigma \tag{25}$$

The chemical shielding is a property that depends on the electronic structure very close to the nuclei. Because of the dependency of the chemical shielding on the electronic structure close to the nuclei, it is not very surprising that relativistic NMR effects are very large for heavy elements.[59] In particular, during the past decade, the computation of NMR shielding based on relativistic methods has been very successful in explaining experimental trends such as the normal and inverse halogen dependence of chemical shifts in classes of compounds as different as organic halides and Pt complexes.

Methods[57] that can calculate chemical shifts of main group elements are now implemented in most standard quantum chemical packages and applied routinely. Figure 8 displays[60] the kind of error one

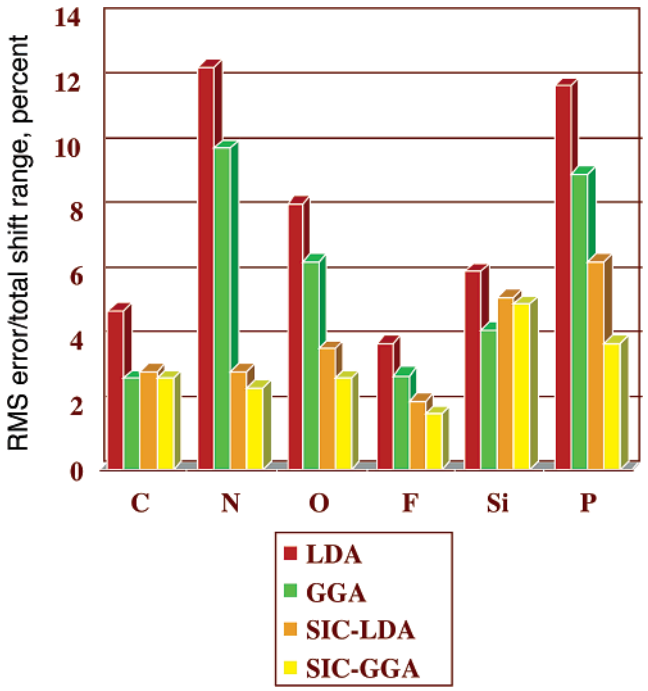

Figure 8. Errors in calculations on chemical shifts for C, N, O, F, Si, and P with LDA and GGA DFT methods with and without SIC.

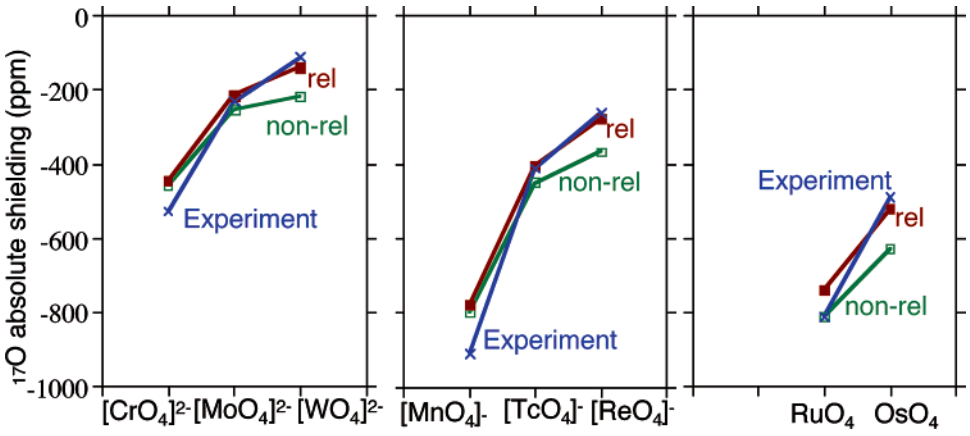

Figure 9. Calculated and observed absolute shielding of ^{17}O in various tetrahedral oxo-complexes $[MO_4]^{n-1}$.

Table 8. ^{13}C Chemical Shifts for Metal−Carbonyls

	d(C−O)[a] (Å)	exp. shift[b]	NR shifts[c]	quasi-rel[d]	quasi-rel + SO[e]
$[Hf(CO)_6]^{2-}$	1.183	244	234	228	235
$[Ta(CO)_6]^-$	1.167	211	216	212	215
$W(CO)_6$	1.152	192	202	198	198
$[Re(CO)_6]^+$	1.139	171	189	184	176
$[Os(CO)_6]^{2+}$	1.127	147	180	172	150
$[Ir(CO)_6]^{3+}$	1.121	121	161	154	126

[a] C−O distances in Å. [b] Experimental chemical shifts from ref 63. [c] Nonrelativistic chemical shifts from ref 63. [d] Quasi-relativistic chemical shift without spin−orbit coupling from ref 63. [e] Relativistic calculations including spin−orbit coupling from ref 63.

Table 9. ^{199}Hg NMR Chemical Shifts

	exp.[a] (ppm)	calcd[b] (ppm)
$HgMe_2$	0.0	0.0
MeHgCl	−810	−711
MeHgBr	−915	−840
$Hg(CN)_2$	−1386	−1508
$HgCl_2$	−1518	−1524
$HgBr_2$	−2213	−2478
HgI_2	−3447	−3412

[a] Experimental shifts, see ref 65. [b] Theoretical shifts, see ref 65.

can expect from various DFT methods. It is clear that chemical shifts due to LDA (rung 1) and GGA (rung 2) have large error bars especially for N, O, and P. These errors can be reduced by resorting to[60] SIC-LDA (rung 4) and SIC-GGA (rung 4) where the self-interaction error inherent in LDA and GGA has been eliminated. For wave function methods, MP2 affords good results for H, C; however, N, O, and P require highly correlated methods such as CCSD(T).[61]

It is of special interest that relativistic effects are important even for lighter elements if these elements are bound to a heavier metal. The point is illustrated in Figure 9 where the shielding of ^{17}O in various tetrahedral oxo-complexes $[MO_4]^{n-1}$ is depicted. It is seen that experiment and nonrelativistic calculations agree well for the 3d and 4d complexes whereas relativistic corrections are required for the 5d complexes.[62] For the oxo-complexes, the dominating relativistic term is the mass increase of the electron as it moves close to the nuclei.

Another case in which the chemical shift of a light element is influenced by a neighboring heavy metal is shown in Table 8, where we provide experimental and calculated[63] ^{13}C chemical shifts for a number of metal hexa-carbonyls. It can be seen that nonrelativistic shift calculations differ considerably from the observed ^{13}C chemical shifts. Adding the relativistic mass effect (quasi-relativistic calculations) does not significantly improve the agreement. A much better agreement is obtained by including spin−orbit coupling. A careful analysis of these and similar calculations reveals that spin−orbit coupling combined with a magnetic field results in a net spin density on the different nuclei, resulting in an additional chemical shift.[64]

The ultimate relativistic effects on chemical shifts are observed for ^{199}Hg, one of the heaviest active NMR nuclei. Table 9 compares calculated[65] and observed ^{199}Hg chemical shifts for a number of two-coordinated Hg(II) compounds. The experimental shift range is quite large from 0.0 ppm in $HgMe_2$ (the reference) to −3412 ppm in HgI_2, and this range is well-reproduced by the calculations. We note further that the chemical shift becomes increasingly negative in the dihalogen series HgX_2 (X = Cl, Br, I). This trend has been attributed to an increasing shielding of the Hg nucleus as the halide becomes less electronegative. In fact, the trend is completely determined by spin−orbit contribution from the X group, which is most important for the heavier iodide group.[65]

6.2. NMR Nuclear Spin−Spin Coupling

In analogy to eq 22, the nuclear spin Hamiltonian describes the interaction between pairs of nuclear spins in a molecule as

$$E = \vec{\mu}_A \vec{\vec{K}}_{AB} \vec{\mu}_B \tag{26}$$

for each pair of nuclei. The reduced indirect nuclear spin−spin coupling tensor for two nuclei A and B in a molecule is in formal agreement with the last equation given by

$$\vec{\vec{K}}_{AB} = \left(\frac{\delta^2 E}{\delta \vec{\mu}_A \, \delta \vec{\mu}_B} \right)_{\mu_A=0;\mu_B=0} \tag{27}$$

As in eq 24, $\vec{\mu}_A$ and $\vec{\mu}_B$ refer to nuclear magnetic

Table 10. Reduced K(M−C) Coupling Constants[a]

molecule	K(M−C) calcd	K(M−C) exp.
$[V(CO)_6]^-$	129	146
$Fe(CO)_5$	220	239
$[Co(CO)_4]^-$	348	380
$Mo(CO)_6$	293	344
$[Nb(CO)_6]^-$	262	319
$[Rh(CO)_5]^-$	713	778

[a] 10^{-19} kg m^{-2} s^{-2} A^{-2}. [b] DFT (rung 2) calculations from ref 67.

moments. The spin−spin coupling is always present in a molecule independent of an external magnetic field but is usually observed in NMR chemical shifts measurements as the fine structure of the spectrum. The rotational average of $\vec{K}_{AB}$ is the reduced constant K_{AB}. Theoretical data for K_{AB} are usually reported in SI units of kg m^{-2} A^{-2} s^{-2} with a typical magnitude of 10^{19}−10^{23}. Experimentally observed are the spin−spin coupling constants J_{AB} in units of Hertz. Their relation to the reduced coupling constants is

$$J_{AB} = \frac{h}{4\pi^2}\gamma_A\gamma_B K_{AB} \qquad (28)$$

Because the J coupling constants depend on the nuclear magnetogyric ratios, comparisons of spin−spin coupling constants for different types of nuclei are more straightforward when referring to the K values instead.

Spin−spin coupling constants between light elements (H, C, N, and O) can be calculated by DFT methods (rung 2 or higher) with good accuracy[66] whereas constants involving fluorine still are problematic. On the other hand,[66] highly correlated methods [CCSD(T)] are required for accurate spin−spin coupling calculations based on wave function methods for the same elements. Metal−ligand coupling constants in complexes of 3d and 4 d elements[67] can be calculated with reasonable accuracy by DFT methods (rung 2) without employing sophisticated relativistic methods (Table 10). However, for metal−ligand coupling constants involving 5d elements, relativistic effects are necessary. This is illustrated in Figure 10 where calculated and observed W−X coupling constants are compared for X = H, F, and C. The comparison is excellent when relativistic effects are included (filled markers) whereas nonrelativistic methods (open markers) afford data in poor agreement with experiment.[68]

Coordination of solvent molecules to the metal has to be taken into account in spin−spin coupling calculations[69] on coordinatively unsaturated metal complexes. This is the case even for such solvents that can be considered as "inert" for chemical shifts. The point is underlined in Table 11 where calculated Hg−C coupling constants are calculated and compared to experiment with two, three, or four solvent molecules coordinated to the metal. The calculated K values are seen to converge to experiment as the first metal coordination sphere becomes saturated. Figure 11 summarizes the good agreement between relativistic DFT calculations and experiment for M−C coupling constants with M = W, Pt, Hg, and Pb after addition of solvent molecules, if required. A more extensive discussion can be found in ref 70.

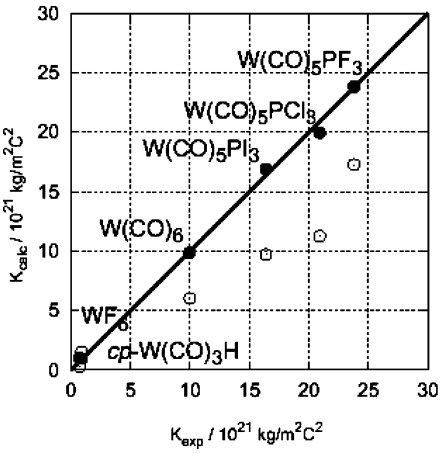

Figure 10. One-bond metal−ligand spin−spin coupling constants (W−C, W−H, and W−F, absolute values) in some tungsten complexes. Data based on nonrelativistic (open markers) and scalar relativistic (filled markers) DFT computations, from ref 68.

Table 11. Computed Hg−C One-Bond Couplings Constants K with 2, 3, or 4 Solvent Molecules Coordinated to Metal

compounds	solvent	+2 solv.	+3 solv	+4 solv.	exp.
HgMeCl	$CHCl_3$	223.5	233.5	277.1	263.1
	DMSO	260.3	295.2		307.8
HgMeBr	$CHCl_3$	218.9	227.2		256.3
	DMSO	253.8	293.6		299.9
HgMeI	$CHCl_3$	192.9	241.2		239.3
	DMSO	251.0	295.4		283.1
$HgMe_2$	$CHCl_3$	108.0	121.8		126.6
	DMSO	118.5	130.7		133.4
$Hg(CN)_2$	MeOH	513.1		560.7	577.8
	THF	511.5		581.8	558.5

[a] 10^{-19} kg m^{-2} s^{-2} A^{-2}. [b] DFT (rung 2) calculations from ref 69 with relativistic effects included.

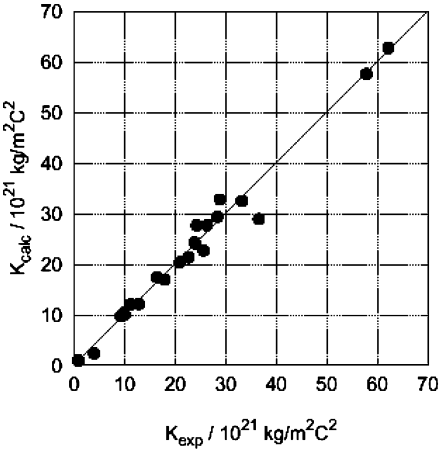

Figure 11. Twenty-three metal−ligand one-bond spin−spin coupling constants in complexes containing W, Pt, Hg, and Pb. Data are based on scalar relativistic DFT computations from ref 68.

6.3 EPR *g*-Tensor

The $\vec{g}$-tensor of electron paramagnetic resonance (EPR) is observed when placing a paramagnetic molecule in an external magnetic field $\vec{B}$. If the effect

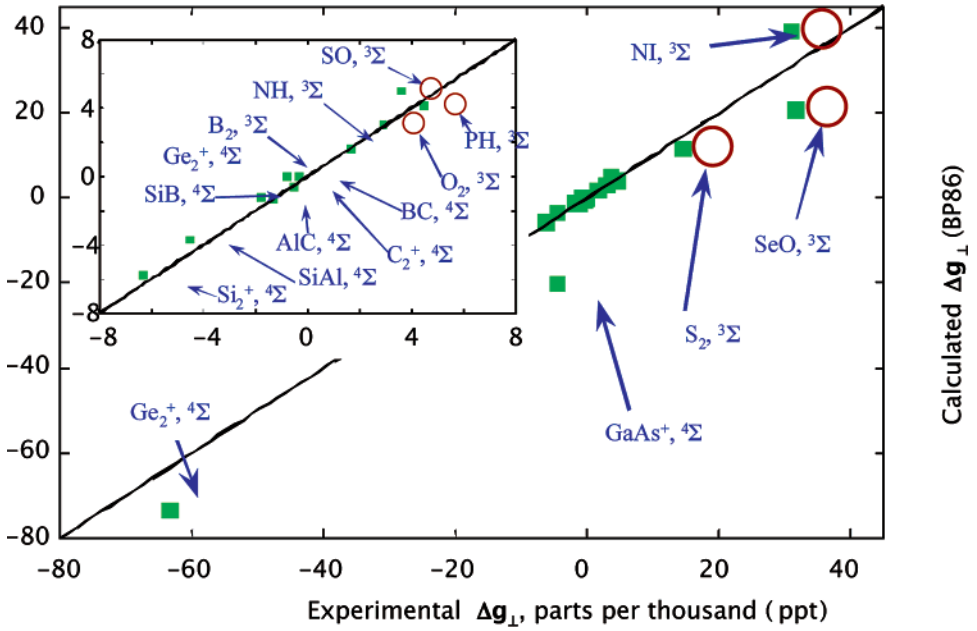

Figure 12. Calculated vs experimental values for a set of mixed main group diatomic high spin radicals, from ref 71c. The $\Delta g_{||}$ values are generally very small and not displayed.

is entirely due to a nonvanishing spin magnetic moment μ_e related to an effective spin vector $\vec{S}$ of the molecule, sometimes the term ESR is preferred. We will entirely focus on the latter here. In analogy to the NMR shielding tensor, the ESR $\vec{g}$-tensor can be defined via an effective spin Hamiltonian that includes the interaction of the electron spins with an external magnetic field and with each

$$\hat{H}^{\text{eff}} = \frac{1}{2}\vec{B}(g + \Delta\vec{g}) \cdot \hat{S} + \hat{S}\vec{D}\,\vec{S} \qquad (29)$$

Equation 29 follows the usual sign conventions for $\Delta\vec{g}$. The eigenvalues of the effective spin Hamiltonian are intended to correspond to the experimentally observed energy levels. D is responsible for a zero-field splitting caused by the electron spin−spin interaction in analogy to the coupling K between nuclear spins, but it can be neglected from the discussion for the limit of a strong external field. The constant g is related to the free electron g-value and can therefore be omitted from the computations. In this case, the $\Delta\vec{g}$-tensor is in formal agreement with the eigenvalues of the spin Hamiltonian of eq 29 given as

$$\Delta\vec{g} = 2\left(\frac{\delta^2 E}{\delta\vec{B}\,\delta\vec{S}}\right)_{\vec{B}=0;\vec{S}=0} \qquad (30)$$

where the derivative with respect to a nuclear magnetic moment in the case of NMR shieldings is replaced here by the derivative with respect to the electronic spin vector $\vec{S}$. The tensor $\Delta\vec{g}$ is dimensionless just as the NMR shielding tensor, and results are typically reported in units of 10^{-6} (ppm) or 10^{-3} (part per thousand, ppt).

Calculations of $\Delta\vec{g}$ tensors for main group elements have been discussed in ref 71. Figure 12 summarizes[71c] results for a number of diatomic main group molecules. The absolute error in the isotropic Δg shifts

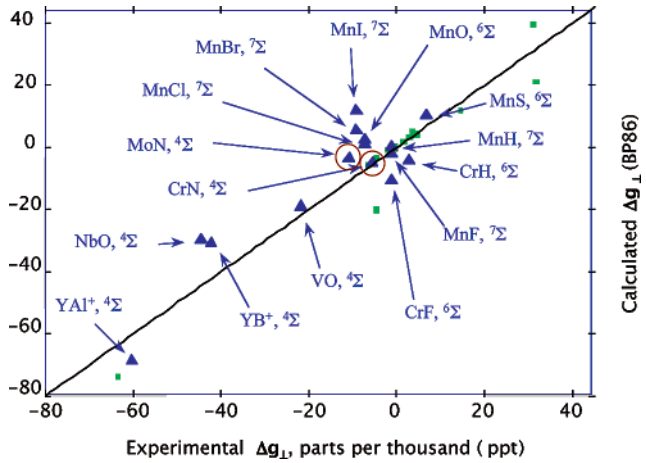

Figure 13. Calculated vs experimental values for a set of mixed main group and transition metal diatomic high spin radicals, from ref 71c. The $\Delta g_{||}$ values are generally very small and not displayed.

is 3.3 ppt where the range of the observed Δg values is −80 to 40 ppt. Figure 13 displays[71c] a comparison between calculated and experimental data for a number of diatomics containing one transition metal and one main group element. This sample is of relevance to transition metal complexes. The absolute error in the calculated isotropic Δg shifts is 6.0 ppt where the range of the observed Δg values is −80 to 40 ppt. Thus, the error in these transition complex models is only slightly higher than in main group compounds.

Transition metal studies[72] have been carried out by Patchkowskii on d^1 complexes of the type MEX_4, with M = V, Cr, Mo, W, Tc, and Re; E = O, N; and X = F, Cl, and Br as well as on $Co(CO)_4$ and $[Fe(CO)_5]^+$ by Malkina[73] et al. Other more recent DFT applications of theoretical methods to $\Delta\vec{g}$ tensors of transition metal complexes include in particular studies on metal porphyrins,[74,75] Fe, Ru, and Os nitrosyl complexes,[76] model complexes for the active center of

[NiFe]-hydrogenase,[77] or biologically relevant vanadyl complexes.[74]

6.4. ESR *A*-Tensor

Another ESR analogue of nuclear spin−spin couplings is the *A*-tensor or hyperfine tensor. The effective Hamiltonian for the interaction of the electronic spin with one of the nuclear spins is[78]

$$\hat{H}_{\text{eff}} = \vec{S}\,\vec{\vec{A}}\,\vec{I}_A \tag{31}$$

As for the properties in previous sections, the *A*-tensor is here in formal agreement with the eigenvalues of eq 31 given as

$$\vec{\vec{A}} = \left(\frac{\delta^2 E}{\delta\vec{I}_{\text{A}}\,\delta\vec{S}}\right)_{\vec{I}_A=0;\vec{S}=0} \tag{32}$$

that is, the effect of the presence of nuclear spin angular momentum on the electronic spin in a molecular environment is investigated. Note that $\vec{\mu}_A = \gamma_A \vec{I}_A$. Equation 32 follows a common convention for the definition of $\vec{\vec{A}}$. Values are typically given in SI units of MHz, or in cgs units of G (Gauss), with a conversion factor of approximately 2.802 MHz/G.[79]

A comprehensive comparison between DFT and coupled-cluster ab initio methods for the computation of *A*-tensors has been carried out recently by Munzarová and Kaupp and is specifically geared toward applications to transition metal complexes.[80] They found that "none of the investigated functionals performs well for all complexes", including hybrid functionals. The coupled-cluster approach did yield very accurate results for the smaller molecules of the test set with a tendency for underestimation of the experimental reference values, but it is still prohibitively expensive for larger systems. The problems with the density functionals have been attributed to difficulties in order to get the correct balance between core spin polarization (which determines the hyperfine coupling constants) and valence spin polarization, which causes problematic spin contamination.[81] The mechanism of ESR hyperfine coupling has been subsequently studied in detail in ref 82 outlining the leading role of overlap between the singly occupied orbital of a doublet system with certain doubly occupied valence orbitals. However, the results were within approximately 10−15% error for most of the complexes and most of the functionals, allowing for a reliable interpretation of the results in comparison with experiments. A similar range of accuracy has also been quoted by Belanzoni[83] et al. where a large set of linear molecules have been studied. In this work, the *A*-tensors have also been analyzed in detail, based on Mulliken populations of the singly occupied molecular orbitals and semiquantitative estimates of the orbital mixing due to spin−orbit coupling. On the basis of elaborate studies of the fluorine *A*-tensor in TiF_3, Belanzoni[84] et al. have also pointed out the difficulties regarding experimental reference values, since often theoretical assumptions are made in order to determine the experimental data. After reconsidering the experimental analysis for TiF_3, good agreement between the theoretical approach[84] and the experiments could be achieved.

6.5. Vibrational Spectroscopy

We have already in section 3.5 discussed how the PES of a molecule of N atoms can be expanded in a Taylor series around a nuclear configuration Q^0. We shall in this section discuss how such an expansion can be used in a theoretical discussion of vibrational spectroscopy.

6.5.1. Harmonic Frequencies

Assuming, to lowest order, a quadratic form for the PES in the vicinity of the equilibrium structure for a molecule, the potential energy U as a function of the mass-weighted nuclear displacements $\Delta\vec{x}_k = (\sqrt{M_k}\Delta X_k, \sqrt{M_k}\Delta Y_k, \sqrt{M_k}\Delta Z_k)$ can be written as

$$U = \frac{1}{2}\,\Delta\vec{x}^{+}\,\vec{\vec{F}}\,\Delta\vec{x} \tag{33}$$

The energy scale has been chosen here such that $U = 0$ when the nuclei are in their equilibrium positions and $\Delta\vec{X}_k$ refers to displacement of atom k from these positions, whereas M_a is the mass of atom a. Finally, $\vec{\vec{F}}$ is the energy Hessian with respect to the mass-weighted nuclear displacements discussed in section 3.5.

$$\vec{\vec{F}} = \left(\frac{\delta^2 U}{\delta\Delta\vec{x}_k\,\delta\Delta\vec{x}_l}\right)_{\Delta\vec{x}_k=0,\Delta\vec{x}_l=0} \tag{34}$$

As mentioned previously, the normal modes $\vec{R}_i$ of eq 14 are the eigenvectors of $\vec{\vec{F}}$ according to eq 1 while its eigenvalues λ_i are the mass-weighted force constants associated with the $\vec{R}_i$. From this, the vibrational spectrum of the molecule in the harmonic approximation can be calculated, since the frequency ω_i of a harmonic oscillation is related to the mass-weighted force constant λ_i by

$$\omega_i = 2\pi\nu_i = \sqrt{\lambda_i} \tag{35}$$

Frequency calculations in the field of transition metal chemistry are not yet fully explored. However, indications[31f,g] are that frequencies are well-represented by standard DFT methods, whereas one must go beyond HF when using wave function methods in order to obtain the same accuracy.

The accuracy of various computational approaches and in particular of DFT for the calculation of harmonic force constants of transition metal carbonyls and carbonyl hydrides has been investigated, e.g., in a series of papers by Jonas and Thiel[31f,85] as well as Berces.[31g] An overview of applications to transition metal complexes is also presented in the DFT textbook of Koch and Holthausen.[86] It was found that DFT performs generally well for such molecules and properties, while HF and MP2 did not yield very satisfactory results. With GGA functionals (rung 2), typical deviations for vibrational frequencies as compared to experiment were found to be in the range of 0−30 cm^{-1} with a tendency to overestimate metal−carbon stretching frequencies and to under-

estimate the C−O stretching frequencies.[85a] Trends for the change in the C−O frequencies upon complexation were also well-reproduced. The remaining errors are well within what one might expect from harmonicity corrections or frequency shifts due to a surrounding matrix. For the carbonyl hydrides, the metal−H stretching frequencies were typically overestimated by 30−50 cm^{-1} for the 3d metals and by 10 cm^{-1} for the other metals.

6.5.2. IR Intensities

The harmonic frequencies discussed in the last paragraph can be combined with a computation of the respective intensities that would be observed for the absorption of an IR light beam of the respective energy in order to simulate IR vibrational spectra. The intensities I_α are (in the double harmonic approximation[87]) proportional to the square of the derivative of the electric dipole moment $\vec{D}$ of the molecule with respect to nuclear displacements along the normal coordinates;[88] that is, this leads to another second energy derivative of the form

$$I_\alpha \propto \left|\frac{\delta \vec{D}}{\delta R_\alpha}\right|^2_{R_\alpha=0} = \left|\frac{\delta^2 E}{\delta R_\alpha \, \delta \vec{E}}\right|^2_{R_\alpha=0;\vec{E}=0} \qquad (36)$$

since the lowest order energy change of a molecule in an electric field $\vec{E}$ is given by $-\vec{D}^0 \cdot \vec{E}$ and, therefore, $\vec{D}^0 = -(\delta E/\delta \vec{E})_{\vec{E}=0}$. The constant of proportionality in eq 36 is $(4\pi\epsilon_o)^{-1}(N_A\pi)/(3c^2)d_\alpha$, with d_α being the degeneracy of the normal mode.[87] IR intensities are usually reported in units of km/mol.

Methods for IR intensity calculations are implemented in most quantum chemistry programs. Several of the aforementioned papers dealing with vibrational spectra of transition metal complexes have therefore also compared the computed intensities to experimental data. Because of certain difficulties in the experimental determination of absolute intensities, often only relative values are given. In ref 89, absolute experimental IR intensities for the strong absorption bands ν_3 of UF_6, NpF_6, and PuF_6 (and also of the weaker ν_4 for UF_6) have been reported. Intensities for UF_6 and PuF_6 could be reproduced by the DFT methods (GGA) within 15% error. An early application of DFT to IR intensities has been carried out in ref 90 for $Ni(CO)_4$ and $Cr(CO)_6$, in good agreement with the available experimental data for both relative and absolute intensities. In case spectra are simulated from theoretical calculations, the usual procedure is to superimpose the calculated line spectrum with Gaussian or Lorentz curves and to directly compare the experimental and the simulated spectrum. Figure 14 displays some simulated IR spectra of metal tris-acetylacetonates, from ref 91. As can be seen, the agreement of the experimental spectra with theoretical predictions is excellent and allows for a complete assignment of the spectra. Because of the good overall agreement, the authors of ref 91 concluded that the experimentally observed band at around 800 cm^{-1} that is not present in the theoretical simulations is not a fundamental frequency. As further examples, Mg and Zn porpyrin spectra have been investigated in ref 92, and Ni porphyrin spectra in ref 93, with similar success in the assignment of the experimental spectra. Limitations in the first principles calculation of IR spectra along with examples have been discussed, e.g., in ref 94. Theoretical approaches, related technical details, and further applications have been reviewed, e.g., in ref 95.

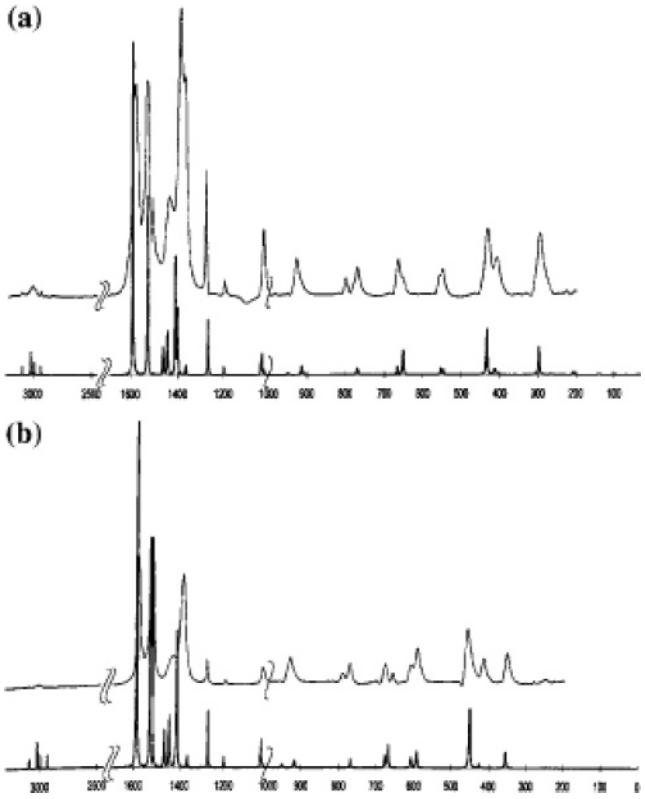

Figure 14. Simulated and experimental IR spectrum of $Fe(acac)_3$ (upper figure) and $Cr(acac)_3$ (lower figure), from density functional calculations, from ref 91; acac = acetylacetonate.

Vibrational modes that are not IR active might be detected by Raman spectroscopy. Raman intensities are calculated by replacing the dipole moment $\vec{D}$ in eq 36 by the polarizability tensor. Calculations of Raman intensities are likely to emerge soon although they are somewhat more expensive[96] to evaluate than IR intensities.

6.5.3. Vibrational Circular Dichroism (VCD)

Chiral molecules will have different IR absorptions for right and left circular polarized light. VCD[97] deals with recording this difference. Applications of first principles theories of VCD have been of considerable interest during the past two decades.[98−100] As with most other properties being discussed so far, more recent developments and applications have concentrated more on DFT because of its computational efficiency. The first calculation for a molecule containing a transition metal has appeared only very recently,[101] employing DFT. The VCD of the complex $Zn(sp)_2Cl_2$, with sp = 6*R*,7*S*,9*S*,11*S*-(−)-sparteine, has been investigated experimentally and by DFT computations (B3LYP). Figure 15 displays the results that have been obtained for the vibrational spectrum. It can be seen that the theoretical results are in good

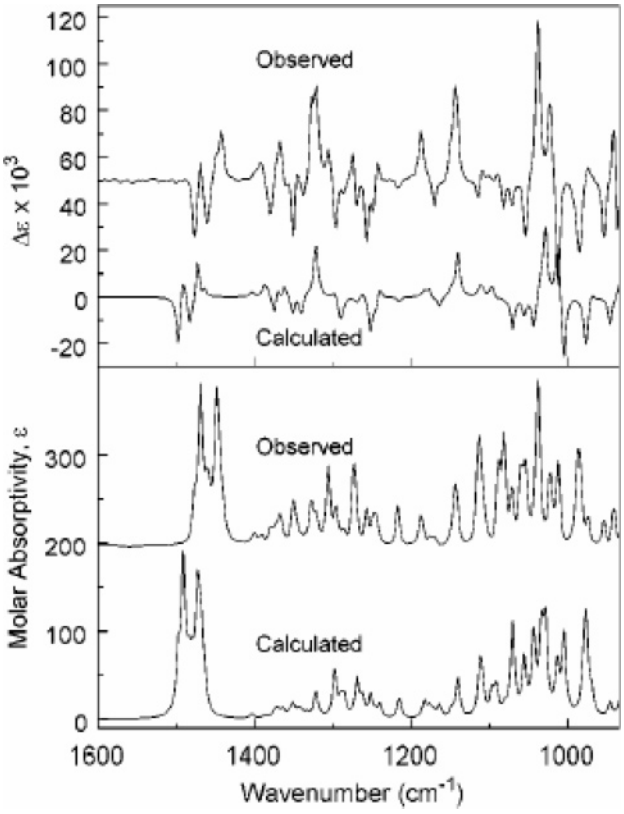

Figure 15. Experimental and calculated (DFT) IR (bottom) and VCD (top) spectra of $Zn(sp)_2Cl_2$, from ref 101. The observed spectra have been offset for better readability.

agreement with the experimental spectra. We briefly note that there exists also corresponding Raman circular dichroism (CD) effects; see, for example, ref 102 for details and literature references.

6.6. UV Spectroscopy

We have already discussed the calculation of electron excitation energies for molecules and transition metal complexes in section 5. These studies can be extended to include intensities of the excitations as well. Intensity calculations are still a field under development, and the agreement with experiment is at best qualitative.[58]

6.6.1 CD and OR

CD is a chirality effect and is observed as the difference $\Delta\epsilon$ of the absorption intensities for left- and right-hand circular polarized light. This difference is related to the OR parameter β that is given theoretically[103] (in Gaussian units) by

$$\beta = \frac{2}{3\hbar}\sum_j \frac{R_{oj}}{(E_o - E_j)^2/\hbar^2 - \omega^2} \qquad (37)$$

where

$$R_{oj} = \mathrm{Im}\,[\langle\Psi_o|\hat{D}|\Psi_j\rangle\langle\Psi_j|\hat{M}|\Psi_o\rangle] \qquad (38)$$

is the rotatory strength for the excitation $o \rightarrow j$. Furthermore, Ψ_o is the ground state with the energy E_o whereas Ψ_j is the wave function for the excited state j with the energy E_j. Also, $\hat{D}$ and $\hat{M}$ are the operators for the electric and magnetic dipoles, respectively, whereas ω is the frequency of the absorbing light.

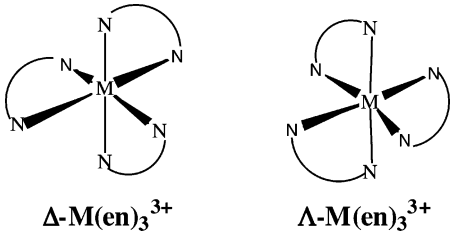

Figure 16. Δ− and Λ− configurations of $Co(en)_3^{3+}$.

Experimentally, the rotatory strength is related to the integrated intensity of the experimentally observed signal $\Delta\epsilon$ for the reference state "0":

$$R_{oj} = \text{const.}\int_{CD\text{Band}j}\frac{dE}{E}\frac{\Delta\epsilon}{l/(\text{mol cm})} \qquad (39)$$

The constant of proportionality in the last equation is approximately 22.97×10^{-40} esu^2 cm^2, referring to cgs units in which the rotatory strengths are usually reported.

Related to CD is optical rotation (OR),[103] the rotation of plane polarized light (a superposition of right- and left-handed polarized light). The macroscopically observed OR is usually reported in experimental work in the form of the specific rotation $[\alpha]_\lambda$ in degrees per (g/cm^3) and per dm (length of the cuvette) for wavelength λ of the perturbing field. Gaussian units are still commonly used in theoretical work related to optical activity, in which case the OR parameter β is in units of cm^4. The conversion factor to specific rotations is then

$$[\alpha]_\lambda = 28800 \cdot \frac{\pi^2 N_A}{\lambda^2 M}\beta(\lambda) \qquad (40)$$

with N_A being Avogadro's number, M the molecular weight in g/mol, and λ the wavelength in cm.

The calculation of ORs and CD by time-dependent DFT has in the past few years received attention from several research groups, and implementations into various codes have been reported quite recently.[104] Methodology involving ab initio codes and earlier semiempirical approaches is described, e.g., in ref 105. We refer also to ref 105 and references therein for more detailed overviews regarding applications to organic molecules, and to ref 106 in particular for an overview of common computational methodology until 1994.

OR and CD for transition metal complexes have been analyzed extensively by semiempirical treatments based on the ligand field model.[107] It allows a qualitative understanding of the CD effect of the lowest energy excitations in terms of small deviations from nonchiral parent symmetries and the associated mixing of orbitals of different parent symmetries upon the chiral distortion of a complex. A very well-studied system[108] is here the complex $[Co(en)_3]^{3+}$ (en = ethylenediamine) and related tri-(bis-amine) complexes of cobalt and rhodium (Figure 16). These systems have recently been the subject of the first[109]

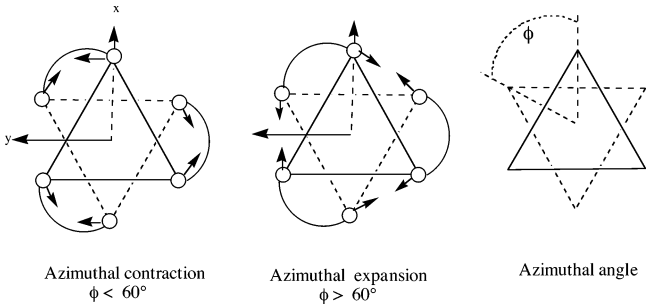

Figure 17. Azimuthal distortion of octahedron.

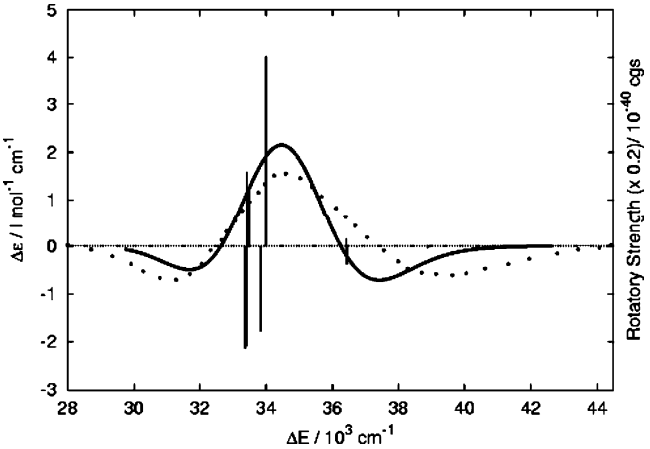

Figure 18. Experimental and simulated CD spectra of Rh(R-pn)$_3$]$^{3+}$. Excitation energies and rotatory strengths are plotted as vertical bars. Experiment (dotted lines) and simulation (solid lines); from ref 109c.

CD study of metal complexes based on TDDFT. It follows from this study that the optical activity of this type of complexes can be related to the azimuthal distortion of the MN_6 framework away from the octahedral geometry (Figure 17). This distortion allows metal t_{2g} type d orbitals to mix with e_u ligand based σ-orbitals.[109b] Figure 18a compares the simulated[109c] and observed CD spectum for $[Rh(pn)_3]^{3+}$ (pn = 1,2-propyl-diamine). The agreement is not quite as good for the corresponding cobalt complexes where d−d transitions are calculated at too high energies whereas ligand-to-metal transitions are calculated at too low an energy.[109] For systems with heavier metals and unsaturated organic ligands, excellent results[109d] can be achieved.

6.6.2. Magnetic CD (MCD) and Magnetic OR (MOR)

In the 1840s, Michael Faraday observed[110] that in the presence of a magnetic field a substance that is optically inactive will rotate plane polarized light. This effect has become known as MOR or the Faraday effect. The magnitude (ϕ) of the MOR induced by a given substance was found to depend on the frequency (ω) of the incident light and to vary linearly with the applied magnetic field ($\vec{B}$). This led to the definition of the Verdet constant, V.

$$\phi = V(\omega) \cdot \vec{B} \tag{41}$$

The transitions of chiral substances have differing absorption coefficients for left and right circularly polarized light $\Delta\epsilon$ and will therefore induce CD as mentioned in the last section. All substances will exhibit CD if a magnetic field is applied parallel to the incident light. This phenomenon is called MCD.

MOR spectra are more difficult to interpret than MCD spectra, and the latter is therefore used significantly more often. A quantitative theory of MCD was derived about 40 years ago[111] in which it was demonstrated that an MCD signal can generally be interpreted in terms of three parameters, which are denoted the A, B, and C terms

$$\Delta\epsilon(o \rightarrow j) = \gamma\left[\mathrm{A}\,\frac{\partial\rho}{\partial\omega} + \left(\mathrm{B} + \frac{\mathrm{C}}{kT}\right)\rho\right] B \tag{42}$$

Here, ρ is the density of state of the frequency ω, and γ is a proportionality constant. Ref 112 contains reviews of earlier work in transition metal chemistry based on ligand-field theory whereas semiemperical studies of organic molecules can be found in ref 113. Relatively few ab initio wave function studies of MOR or MCD have been reported. The majority of publications have dealt with calculations of the Verdet constant of small molecules,[114] whereas only a few studies of MCD parameters have appeared. DFT formulations for the Verdet[115] term as well as the A[116] and C[117] terms of MCD are also emerging.

7. Determination of Reaction Rates from PESs

Observed reaction rates are macroscopic averages over a large number of "chemically identical systems" passing with diverse initial velocities from the reactant valley to the product valley along different trajectories. Thus, to determine the rates, one must either perform a large number of trajectories in an approach based on dynamics or introduce statistical theories based on ensemble distributions. This section will deal with dynamical approaches whereas statistical theories will be discussed in the next section.

In classical dynamical approaches, the reaction rate for a chemical calculation is determined by averaging[118] a statistically representative number of trajectories with different initial conditions that brings "the same chemical system" from reactant to product.

In the classical trajectory calculations, the nuclei are allowed to move on the potential surface according to Newton's classical laws of motion (eq 43)

$$m_i \frac{\partial^2 \vec{X}_i}{\partial t^2} = -\frac{\partial U(\vec{X}_1, \vec{X}_2, \ldots, \vec{X}_i, \ldots \vec{X}_N)}{\partial \vec{X}_i} \tag{43}$$

where $i = 1, 2 \ldots N_{\mathrm{nuc}}$. Thus, the position $\vec{x}_i(t + \Delta t)$ of nucleus i at time $t + \Delta t$ can be deduced from the position, velocity, and force at t as

$$\vec{X}_i(t + \Delta t) = \vec{X}_i(t) + \frac{\delta \vec{X}_i(t)}{\delta t}\Delta t - \frac{1}{2m_i}\frac{\delta U}{\delta \vec{X}_i}\Delta t^2 \tag{44}$$

It is thus possible in a number of time steps (Δt) to propagate the system from reactant to product. We shall refer to the literature for the exact way in which a statistically representative number of trajectories are selected as well as how they are averaged to

produce a reaction rate.[119] However, we shall in the following discuss how one in practice obtains the potential energy gradients $\delta U/\delta \bar{X}_i$ required to propagate the trajectories according to eqs 43 and 44.

7.1. Classical Trajectories with Fitted PESs Based on Empirical Force Fields or ab Initio Calculations

The first chemical trajectory calculations were based on empirical PESs.[120] Of special historical importance has been the LEPS[120] (London−Eyring−Polanyi−Sato) surface for triatomic molecule. The LEPS was used in the period from 1950 to 1980 to develop many of the basic concepts of MD. In more recent years, generalized empircal potentials for chemical reactions have been developed by Rappé[121] et al. The potential by Rappé can be used even for transition metals and holds great promise for large systems including metal surfaces.

Within the past 20 years, empirical force fields for small systems have given way to PESs obtained by fitting[122] data generated[123] by high level ab initio wave function methods. The new potentials for triatomic ($O + H_2$, $Cl + HCl$, $H + H_2$, etc.) and a few four-atom systems ($H_2 + H_2$, $OH + H_2$, etc.) make it possible to test quantitatively kinetic rate theories against highly accurate experimental measurements. Unfortunately, fitting multidimensional functions with more than four nuclei is a formidable and in practice intractable task. This method has as a consequence not been used much for inorganic systems. Fortunately, alternatives to methods based on fitted potential surfaces do exist as we shall show in the next section.

7.2. Classical Trajectories from ab Initio Energy Gradients

As an alternative to fitting the PES to ab initio data, the energy gradient $-dU/dX$ (eqs 43 and 44) needed to determine the position at $\vec{x}_i(t + \Delta t)$ (eq 44) can be calculated directly by ab initio methods. This procedure has been termed direct dynamics.[124] It requires a full electronic structure calculation in which the expansion coefficients of eq 9 $\{C_{ik};i = 1,n;k = 1,m\}$ are fully optimized for each time step, Δt. Because some 10 000−50 000 time steps are required in one trajectory, this method is still too expensive for all but the smallest of systems. The propagation of the atoms on a potential surface according to eqs 43 and 44 is often referred to as MD.

Direct dynamics[125] has been carried out on a large number of reactions involving main group elements with up to 15 atoms by Gordon,[125] Hase,[126a] Sun,[126b] and many others. The method has in addition been extended to excited states and photochemical reactions.[127] Of particular interest here is the study of photodissociation by a CO ligand from chromium hexacarbonyl by Robb et al.,[128] which is one of the first applications of direct dynamics to transition metal complexes. There have been several recent attempts to speed up direct dynamics calculations;[129] these developments hold the promise that direct dynamics can be applied to larger systems.

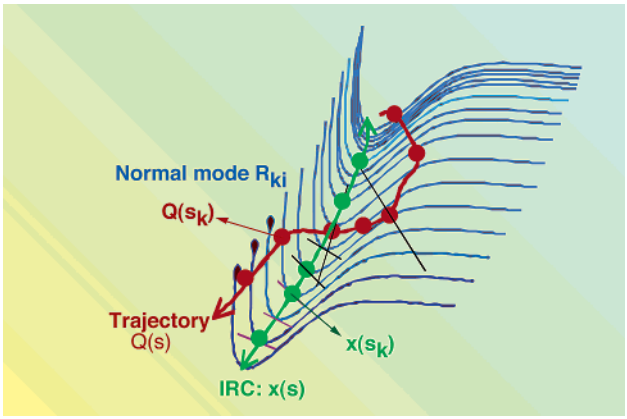

Figure 19. Decomposition of a trajectory (red line) into motions along the IRC (green line) and normal modes perpendicular to the IRC.

A powerful tool for analysis of results from direct dynamics has been provided by Miller et al.[130] in the form of the reaction path Hamiltonian approach (RPHA). The RPHA can be used[131] to analyze trajectories that follow the valley around the IRC discussed in 3.62; see also Figure 19. A given point $\bar{Q}_k(\bar{X}_{k,1},\bar{X}_{k,2},...,\bar{X}_{k,i},\bar{X}_{k,j},...,\bar{X}_{k,3N})$ along a trajectory is described in terms of a point on the IRC given by $\vec{x}(s_k)$, see eq 20, and the $3N - 7$ normal modes $\bar{R}_{ki}$ perpendicular to the IRC as well as the total rotation $\bar{L}_k$ and translation $\bar{T}_k$. The total energy is partitioned according to a harmonic analysis into potential and kinetic energy of the coordinates $\vec{x}(s_k),\bar{R}_{ki}$ $(I = 1,3N - 7)$, $\bar{L}_k$, and $\bar{T}_k$. As the system progresses along the trajectory $\bar{Q}_k$ $(k = 1,n)$, one can now study how energy flows between the different degrees of freedom $\vec{x}(s_k),\bar{R}_{ki}$ $(I = 1,3N - 7)$, $\bar{L}_k$, and $\bar{T}_k$ as k changes. The RPHA is a natural extension of the IRC analysis at $T = 0$ K to finite temperatures.

7.3. Classical Trajectories from ab Initio Theory Based on the CP Method

In 1985, Car and Parrinello[132] developed a direct dynamics scheme in which the orbital coefficient $\{C_{ik};i = 1,n;k = 1,m\}$ formally is considered as dynamic quantities with fictitious masses μ and propagated in time according to

$$\mu \ddot{c}_{i,k} = -\frac{\partial U}{\partial c_{i,k}} - \sum_j \lambda_{i,j}\, c_{i,k} \qquad (45)$$

parallel to the nuclear positions according to eq 45.

Formally, the nuclear and electronic degrees of freedom are cast into a single, combined Lagrangian:

$$L = \frac{1}{2}\sum_{i=1}^{n} \mu_i \left\langle \frac{\delta \varphi_i}{\delta t} \middle| \frac{\delta \varphi_i}{\delta t} \right\rangle + \frac{1}{2}\sum_{l=1}^{l=N} m_l \frac{\delta \vec{x}_l}{\delta t} \cdot \frac{\delta \vec{x}_l}{\delta t} - E(|\varphi_i\rangle,\vec{x}_l) + \sum_{i,j} \Lambda_{ij} \langle \varphi_i \mid \varphi_j \rangle \qquad (46)$$

where the first two terms represent the kinetic energy of the wave function and nuclei, respectively, the third term is the potential energy, and the last term accounts for the orthogonality constraint of the orbitals. If the fictitious masses are such that the

fictitious kinetic energy of the wave function is very small as compared to the physically relevant kinetic energy of the nuclei, then the CP method propagates the electronic configuration very near to the proper Born−Oppenheimer surface. The generated electronic structure oscillates around the Born−Oppenheimer surface, which over time gives rise to stable MD. The coupled CP dynamics, therefore, results in a speed up over conventional direct dynamics since the electronic wave function does not have to be converged at every time step; instead, it only has to be propagated. The primary disadvantage of the CP scheme is that the electronic configuration oscillates about the Born−Oppenheimer wave function at a high frequency. Therefore, to generate stable MD, a very small time step must be used, usually an order of magnitude smaller than in conventional ab initio MD. The CP method has been use to study the trajectory from the TS to the products and reactants in a number of organometallic reactions.[133] Such studies are highly informative but do not provide quantitative information about reaction rates due to the limited number of studied trajectories. The CP method has been extended to include QM/MM[134] and the COSMO[135] solvation model. The CP method is an example of an ab initio molecular dynamics (AIMD) method since no empirical input is needed.

The CP method was initially implemented into programs based on plane waves where the energy gradient can be evaluated very efficiently. Unfortunately, for larger systems, the number of plane waves increases as L,[3] where L is the length of the unit cell used in the plane wave calculation. To avoid this unfavorable scaling, Hutter[136] et al. have recently developed a CP scheme based on regular atom-centered Gaussian basis functions, which promise to be faster than plane wave CP methods for larger systems.

7.4. Quantum Dynamics with Fitted PESs

Quantum dynamics makes use of the time-dependent Schrödinger equation for a system

$$-\frac{\hbar}{\mathrm{i}}\frac{\partial\Psi}{\partial t} = -\sum_{i=1}^{i=N}\frac{\hbar^2}{2m_i}\nabla^2\Psi + E\Psi \qquad (47)$$

of N nuclei with the potential energy E. The method is only feasible for up to three nuclei. However, for larger molecules, the remaining degrees of freedom can be treated as "background". Quantum dynamics has been used extensively for hydrogen-containing systems where tunneling might be of importance. Examples from inorganic chemistry are absorption of H_2 on metal surfaces,[137a] exchange of hydrogen between hydride and dihydrogen ligands[137b] in transition metal complexes, and photodissociation of H_2[137c] or H[137d] from metal complexes. It is likely that this method will be used extensively to probe quantum effects in processes involving hydrogen atom transfer[137e] where quantum effects such as tunneling will be especially important.

8. Determination of Reaction Rates from PESs Using Statistical Approaches

The most well-known statistical approach to the calculation of reaction rates is the TS theory by Eyring[138b] in which the degrees of freedom perpendicular to the RC at the TS are assumed to be in thermal equilibrium with degrees of freedom of reactants and products. The rate constant for reactions in the condensed phase can according to the TS theory by Eyring be written as

$$k = \kappa\frac{k_B T}{\hbar}\exp[-\Delta G^{\#,0}(T)/RT] \qquad (48)$$

where $\Delta G^{\#,0}$ is the standard state free energy of activation, k_B is the Boltzmann constant, $\hbar$ is Plank's constant, and κ is the transmission constant. The κ factor takes into account the probability of trajectory recrossing over the TS ridge as well as nonequilibrium and quantum effects. However, it is often taken as $\kappa = 1$. We shall in the following discuss how the TS theory is used in practical calculations.

8.1. TS Theory Based on the Harmonic Approximation

In conventional TS theory, $\Delta G^{\#,0}$ is evaluated[138b] at the saddle point of the PES of the reaction (Figure 1) using standard expressions from statistical mechanics[138a] based on the relative energies, vibrational frequencies, total masses, and moments of inertia of reactants, TSs, and products. The vibrational frequencies are readily available from electronic structure calculations within the harmonic approximation.[138a] In the variational transition state theory (VTST) by Truhlar,[138b] $\Delta G^{\#,0}$ is taken at the top of a minimum free energy path that connects reactants and products rather than at the top of the MEP. However, the extra cost has so far prevented the application of VTST to transition metal complexes.

A systematic study on the performance of different theoretical methods with respect to the calculation of activation barriers and free energy of activation is available for organic reactions[139] but not yet for inorganic processes. The most extensive evaluations are on coordinatively unsaturated metal ions attached to a single organic molecule[140a,b] or ligand.[140c] However, these seemingly simple systems have an electronic structure that is much more complex than larger coordinatively saturated complexes. Some comparisons between theory and experiment have been carried out for ligand substitution processes in octahedral[141] and square planar complexes,[142] migratory insertion of CO[137b] and ethylene[143] into metal−alkyl bonds, and oxidative addition of H−H[144a] and H−C[144b] bonds to metal centers. The picture emerging from the limited data is similar to that reached for thermodynamic properties.[9c] Thus, among the wave function methods, CCSD(T) is required for 3d elements to obtain accurate barriers (±5 kcal/mol) whereas the lower level MP2 theory can be used in some cases for 4d and 5d elements. For DFT, the GGA schemes (PB86 and RPBE) as well as B3LYP afford in most cases kinetic barriers within 5 kcal/mol.

A number of excellent review papers have already appeared on the application of first principle methods to inorganic reactions based on the Eyring TS theory. They cover studies on ligand substitution reactions,[145] insertion reactions,[145,146a] oxidative addition,[145,146b,e] nucleophilic[145a] and electrophilic[145a] attack, as well as metallacycle formation[146c,146d] and surface chemistry.[147] Reviews are also available on application to homogeneous[148a] and heterogeneous[148b,c] catalysis as well as metalloenzymes.[148d−f]

The thermal rate constant of a chemical reaction can be calculated using VTST in conjunction with IRC,[149] and dynamic properties can also be obtained by means of analyzing the curvature along the IRC, based on the RPHA due by Miller[131] et al.

8.2. TS Theory Based on Thermodynamic Integration

The harmonic approximation used above is excellent in many cases. However, for processes where weak intermolecular forces dominate, the harmonic or quasi-harmonic approximation breaks down.[150] In these cases, AIMD simulations can be utilized to determine reaction free energy barriers. An MD simulation samples the available configuration space of the system in order to produce a Boltzmann ensemble from which a partition function can be constructed and used to determine the free energy. However, finite MD simulations can only sample a restricted part of the total configuration space, namely, the low energy region. Because estimates of the absolute free energy of a system require a global sampling of the configuration space, only relative free energies can be calculated.

A number of special methodologies have been developed to calculate relative free energies. Because we are interested in reaction free energy barriers, the method of choice is derived from the method of thermodynamic integration.[151] Assuming we are sampling a canonical NVT ensemble, the Helmholtz free energy difference, ΔA, between an initial state with $\lambda = 0$ and a final state with $\lambda = 1$, is given by eq 49.

$$\Delta A_{(0\rightarrow 1)} = \int_0^1 \frac{\partial A(\lambda)}{\partial \lambda}\, \mathrm{d}\lambda \tag{49}$$

Here, the continuous parameter λ is such that the potential $E(\lambda)$ passes smoothly from initial to final states as λ is varied from 0 to 1. Because the free energy function can be expanded in terms of the partition function:

$$A(\lambda) = -kT \ln\left[\int\cdots\int \exp\left[-\frac{E(\vec{X}^N,\lambda)}{kT}\right] \mathrm{d}\vec{X}^N\right] \tag{50}$$

the relative free energy ΔA can be rewritten as

$$\Delta A_{(0\rightarrow 1)} = \int_0^1 \left(\int\cdots\int \frac{\partial E(\vec{X}^N,\lambda)}{\partial \vec{\lambda}}\, \mathrm{d}\vec{X}^N\Big|_\lambda\right) \tag{51}$$

or

$$\Delta A_{(0\rightarrow 1)} = \int_0^1 \left\langle \frac{\partial E(X^N,\lambda)}{\partial \lambda}\right\rangle_\lambda \mathrm{d}\lambda \tag{52}$$

where the subscript λ represents an ensemble average at fixed λ. Because the free energy is a state, function λ can represent any pathway, even nonphysical pathways. However, the ideal choice is the MEP. The RC can be sampled with discrete values of λ on the interval from 0 to 1 or carried out in a continuous manner in what is termed a "slow growth" simulation[149a] by

$$\Delta A = \sum_{i=1}^{N_{\mathrm{steps}}} \left\langle \frac{\partial E(\lambda)}{\partial \lambda}\right\rangle_i \Delta\lambda_i \tag{53}$$

where i indexes the step number. Here, the free energy difference becomes the integrated force on the RC. It can be thought of as the work necessary to change the system from the initial to final state. The discrete sampling resembles a linear transit calculation such that a series of simulations is set up corresponding to successive values of the RC from the initial to final state. For each sample point, the dynamics must be run long enough to achieve an adequate ensemble average force on the fixed RC. In a slow growth simulation,[151a] the RC is continuously varied throughout the dynamics from the initial to the final state. Thus, in each time step, the RC is incrementally changed from that in the previous time step.

Margl and co-workers have pioneered the use of the slow growth method in studies of reactions involving metal complexes with AIMD. These studies include C−H activation[152a] of methane by a Rh(I) complex, CO insertions into metal−alkyl bonds,[60b,152b] olefin insertion into the metal−ethyl bond of $Cp_2Zr(C_2H_5)^{(+)}$[152c] and $(CpSiH_2NH)Ti-(C_2H_5)^{(+)}$,[152d] chain termination in $(CpSiH_2NH)Ti-(C_2H_5)^{(+)}$,[152e] formation of dihydrogen allyl complex from $CpSiH_2NH)Ti-(C_2H_5)^{(+)}$,[152f] and olefin complexation to Ni(II).[152g] The application of the slow growth method to transition metal complexes has been reviewed.[152h−j] The slow growth method has been extended to include QM/MM[147a] and the COSMO[147b] solvation model. Both discrete sampling[153a] and slow growth[153b] are ideally suited to simulate explicit solvation.

8.3. Importance of Entropic Effects

The ability to trace not only the PES but also the free energy profile of a reaction has led to a better understanding of the role played by entropy in chemical reactions.

One such case is the bimolecular reactions between a Lewis acid A (e.g., BH_3) and a Lewis base B (e.g., H_2O) to form the adduct AB, a reaction category that is common throughout chemistry.[154] A plot of the energy profile $U(R)$ as a function of the distance R between A and B reveals for a number of these reactions[154] a decrease in energy from reactants to product without an energy barrier corresponding to a TS as illustrated in Figure 20. However, adding new entropic effects $[\Delta S(R)]$ to produce the free energy profile $\Delta A(R) = \Delta U(R) - T\Delta S(R)$ results at a sufficiently high temperature in a barrier. This can be undertood by observing that $\Delta S(R)$ decreases as AB is formed due to the loss of rotational and

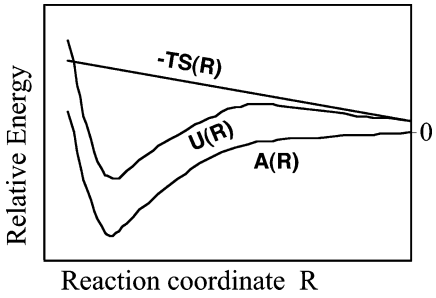

Figure 20. Decomposition of the free energy profile $\Delta A(R) = \Delta U(R) - T\Delta S(R)$ into the potential energy $\Delta U(R)$ and the entropic contribution $-T\Delta S(R)$ for the reaction A + B → AB.

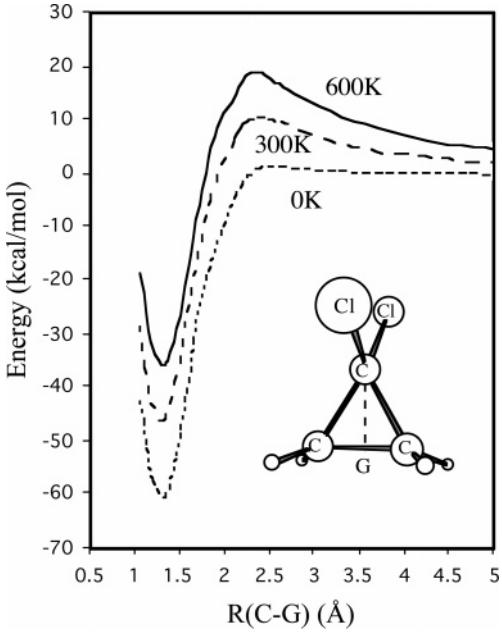

Figure 21. Energy profile the cyclopropanation reaction between CCl_2 and ethylene at 0, 300, and 600 K.

translational entropy. As a consequence, $-T\Delta S(R)$ will increase as AB is formed, leading to a barrier and associated TS on the free energy profile.

Figure 21 illustrates the points made above in a concrete example taken from the reaction between CCl_2 and ethylene to produce dichloro-cyclo-propane. At 0 K, corresponding to the PES, this process does not have a barrier. However, at 300 K, a barrier of 10 kcal/mol has emerged, which increases to 20 kcal/mol at 600 K. In addition, the position of the barrier is seen to move from $R = 2.40$ Å at 300 K to 2.33 Å at 600 K, where R is the distance between the midpoint of the olefin bond and the carbene carbon. Thus, we notice that the TS structure is temperature-dependent with a tendency to move toward the product at higher temperatures. A related example can be found in a recent study of enantioselective cyclopropanation catalyzed by copper complexes where the process responsible for the selectivity only has a barrier on the free energy surface.[155]

Another catalytic example comes[152g] from the polymerization of ethylene by the Ni(II)-based diimine Brookhart complex shown in Figure 22. The very first step in the polymerization process is the uptake of an ethylene molecule to form a olefin π-complex as shown in Figure 22. The calculation of the potential

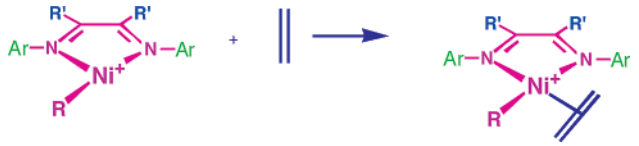

Figure 22. Uptake of ethylene by the Brookhart catalyst.

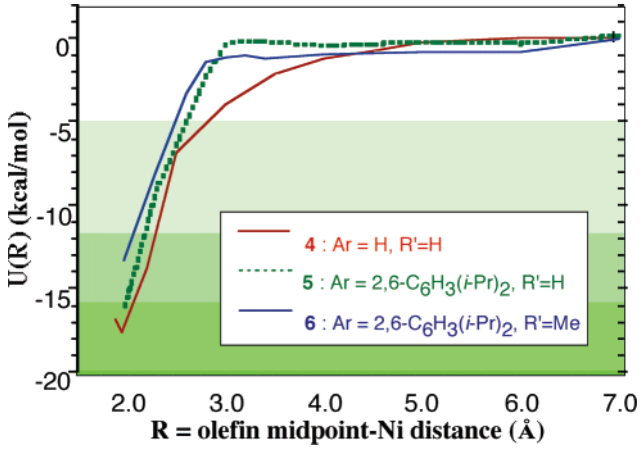

Figure 23. PES for uptake of ethylene by three different Brookhart catalysts.

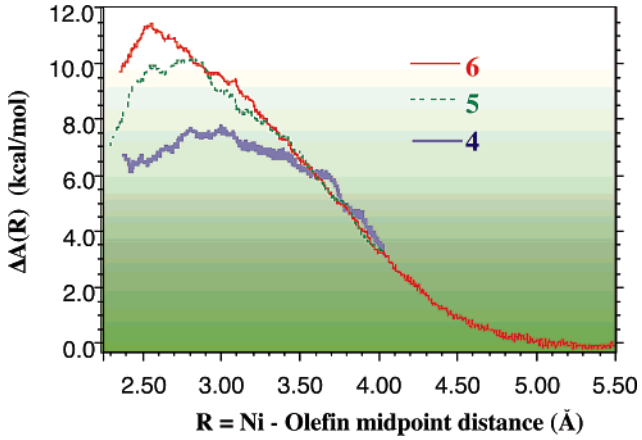

Figure 24. Free energy surface for uptake of ethylene by three different Brookhart catalysts.

energy profile for three different ligand sets: (1) R′ = H, Ar = H (red); (2) R′ = H, Ar = 2,6-C_6H_3(i-Pr)$_2$ (green); and (3) R′ = CH_3, Ar = 2,6-C_6H_3(i-Pr)$_2$ (blue) reveals no barrier (Figure 23). However, as the entropic term is added at 300 K, we see for all three systems a clear barrier (Figure 24). Thus, the ethylene uptake barrier is completely entropic in nature.

It is also possible that the reaction mechanism changes from the PES to the free energy surface. Such a case has recently been discussed by Yang[156] et al. in a study on the degenerate substitution reaction

$$*NH_3 + H_3BNH_3 \rightarrow H_3B*NH_3 + NH_3 \quad (54)$$

This reaction has a potential energy profile where the incoming NH_3 hydrogen binds to the complexed NH_3, A and A′ of Figure 25. As the reaction progresses further on, an encounter complex is formed, B and B′ of Figure 25, with the NH_3 units on each side of the boron atom. Finally, a symmetrical TS is reached, TS of Figure 25, that is typical of a S_N2 substitution

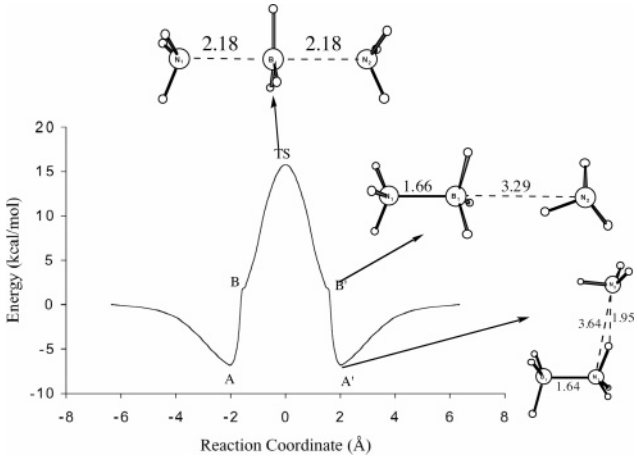

Figure 25.

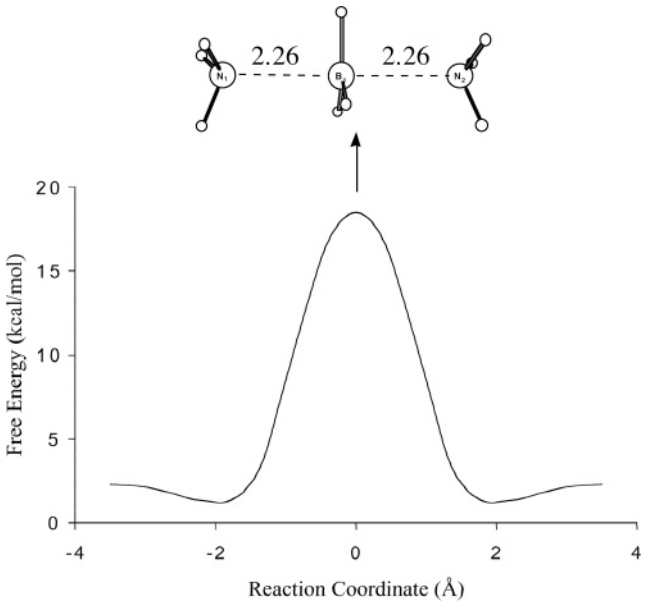

Figure 26. PES for $N^*H_3 + H_3BNH_3 \rightarrow H_3BN^*H_3 + NH_3$ as a function of RC = R(B − N) − R(B − N*).

reaction. At 300 K, the free energy profile reveals that B and B′ have disappeared and that A and A′ at best exist as a shallow minimum. The process still has a symmetrical TS typical of a S_N2 substitution reaction. However, the two B−N distances have increased from 2.18 Å at 0 K to 2.26 Å at 300 K (Figure 26). The comparison between the profiles at 0 and 300 K underlines that some of the shallow minima present on the PESs might be "washed out" by temperature effects. Finally, moving on to 600 K, we note that the symmetrical TS has disappeared. Instead, we now have two asymmetrical TSs A and A′ (Figure 27), in which one NH_3 unit is entering to displace the NH_3 unit bound to boron as shown in Figure 28, where we display the two B−N distances along the RC. After the TS, a symmetrical intermediate is reached. However, the "intermediate" corresponds to a point where we have two NH_3 molecules and one BH_3 all separated (Figure 28). Thus, the mechanism has changed to a S_N1 type substitution aided to some degree by a NH_3 molecule.

The exploration of the free energy surfaces is likely to be greatly aided by the recent development of methods that can calculate the free energy gradient.[157] Such a methodology will make it possible to optimize free energy structures for TSs, reactants, and products in much the same way that it has been done on the PES in the past.

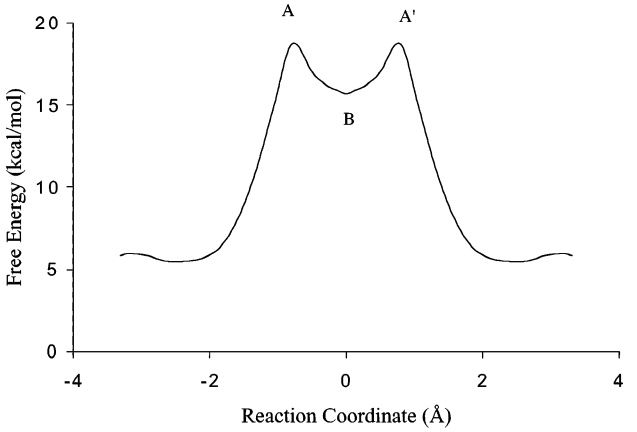

Figure 27. Free energy surface at 300 K for $N^*H_3 + H_3BNH_3 \rightarrow H_3BN^*H_3 + NH_3$ as a function of RC = R(B − N) − R(B − N*).

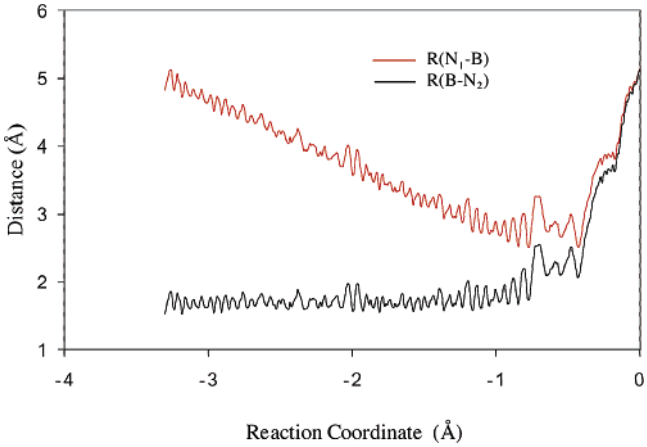

Figure 28. Free energy surface at 300 K for $N^*H_3 + H_3BNH_3 \rightarrow H_3BN^*H_3 + NH_3$ as a function of RC = R(B − N) − R(B − N*).

9. Concluding Remarks

Electronic structure theory has over the past 10 years progressed to the point where it is possible to describe the PES of a gas phase molecule containing up to 10 atoms with great accuracy using high level wave function methods such as CCSD(T) (ground state) or CASPT2/SAC-CI (excited states). For larger systems, acceptable accuracy can be obtained by DFT (ground state) or TD-DFT/ΔSCF-DFT (excited states). Great strides have also been taken in describing the PES for reactions on surfaces[147a] in the interface between gas phase and solid state. Here, DFT will continue to be the electronic structure theory of choice.[19b] Of special importance for transition metals is the development of methods that include relativistic effects since they are required to describe periodic trends correctly within a triad of transition metals. As hardware becomes faster, larger molecules can be treated with higher accuracy using existing methodology. Known methods are also likely to become faster by neglecting interactions between fragments in large molecules that are "far apart". In

this way, most methods will eventually become linear[8] in the number of atoms if this number is large enough. It is finally possible that further progress in approximate DFT will result in new methods with the same accuracy as highly correlated wave functions and speeds still comparable to GGA-DFT.

Many chemical systems of interest have large bulky groups that exert steric pressure on the reactive center (Figure 6) as an essential part of how they function. For such systems, increasing use will be made of dual- or multilevel approaches in which the steric bulk is treated at a lower level of theory than the reactive system.[36,37] The reason that one would like to treat bulky groups by MM is not only that they have a large number of electrons but also (rather) that they potentially possess a formidable number of conformations. The many conformations make it difficult (expensive) to determine the global energy minimum even with MM.

Solvent effects can have a profound influence on chemical reactions; yet, we do not at the moment have a proven methodology (as in the case of electronic structure theory) that by well-known routes can converge to chemical accuracy. Continuum methods[39,41] are going to carry the bulk of the workload in the foreseeable future. However, it will be one of the major challenges within the next decade to develop solvation theories that by standard procedures will converge to chemical accuracy.[41b] Such methods are likely to combine explicit solvation for the first few solvation shells with bulk descriptions (continuum or mean-field[158]) for the remaining part of the solvent.[43,47]

Turning next to dynamics on the PES and calculations of reaction rates, one might expect that these rates for the majority of cases will be determined with the help of Eyring's TS method. To this end, locating saddle points on the PES is still time consuming in terms of manpower, and more systematic and automated procedures would be welcome.[32]

The standard applications of Eyring's TS method make use of a saddle point along the MEP (the TS) as well as frequencies based on the harmonic approximation. Thus, standard applications will not be possible for reactions without an enthalpic barrier (most radical recombination processes and acid base reactions[151g]) or for reactions with many low frequency modes (such as processes in solution with several explicit solvent molecules included, nucleation, and folding of large molecules). In those cases, the free energy of activation will have to be determined from methods based on thermodynamic integration[74] and the variational TS method.[138b] Finally, for reactions involving light atoms such as hydrogen tunneling, effects will have to be taken into account.[137]

For the dynamical motion on excited state surfaces, one has to deal with adiabatic crossings from one PES to another in problems related to photochemistry and electron transfer. This area is still under development with new promising theories[159a] and implementations/applications.[159b] The status of dynamic calculations on PES's has recently been reviewed.[159c]

The number of studies of inorganic reaction mechanisms by theoretical methods has increased drastically in the past decade. The studies cover ligand substitution reactions,[145] insertion reactions,[145,146a] oxidative addition,[145,146b,e] nucleophilic[145a] and electrophilic[145a] attack, as well as metallacycle formation[146c,d] and surface chemistry,[147] in addition to homogeneous[148a] and heterogeneous[148b,c] catalysis as well as metalloenzymes.[148d–f] We can expect the modeling to increase further both in volume and in sophistication.

10. Acknowledgment

We thank the present or former students L. Fan, L. Versluis, T. K. Woo, K. Vanka, J. Cooper, I. Hristov, L. Deng, E. Kelly, and E. Zurek as well as former or present PDF's A. Michalak, M. Seth, P. Margl, R. Schmid, H. M. Senn, S. Tobisch, T. Firman, P. Fleurat-Lessard, S. Y. Yang, F. Wang, and D. Deubel. This work was supported by the Natural Sciences and Engineering Research Council (NSERC). T.Z. also thanks the Canadian Government for a Canada Research Chair in Theoretical Inorganic Chemistry. J.A. is grateful for financial support from the Petroleum Research Fund and the National Science Foundation, and thanks the Deutsche Forchungsgemeinschaft for an Emmy Noether Fellowship in 2003.

11. References

(1) (a) Jordan, R. *Reaction Mechanisms of Inorganic and Organometallic Systems*; Oxford University Press: Oxford, 1991. (b) Atwood, J. D. *Inorganic and Organometallic Reaction Mechanisms*; VCH: New York, 1997.
(2) Shriver D. F. *Coord. Chem. Rev.* **1990**, *99*, 3.
(3) Ford, P. C. *Coord. Chem. Rev.* **1999**, *187*, 3.
(4) Levine, I. R. *Quantum Chemistry*, 5th ed.; Prentice Hall: New Jersey, 2000.
(5) (a) Dewar, M. J. S. *Adv. Chem. Phys.* **1965**, *8*, 65. (b) Woodward, R. B.; Hoffmann, R. *The Conservation of Orbital Symmetry*; Verlag Chemie: Berlin, 1970. (c) Pearson, R. G. *Symmetry Rules for Chemical Reactions*; John Wiley and Sons: New York, 1976. (d) Albright, T. A.; Burdett, J. K.; Whangbo, M.-H. *Orbital Interactions in Chemistry*; John Wiley & Sons: New York, 1985. (e) Fukui, K. *Acc. Chem. Res.* **1971**, *4*, 57.
(6) Glasstone, S.; Laidler, K. J.; Eyring, H. *The Theory of Rate Processes*; McGraw-Hill: New York, 1941.
(7) (a) Hilliers, I. H.; Saunders, V. R. *Chem. Commun.* **1969**, 1275. (b) Demuynck, J.; Veillard, A. *Chem. Phys. Lett.* **1970**, *6*, 204.
(8) Ochsenfeld, C.; White, C. A.; Head-Gordon, M. *J. Chem. Phys.* **1998**, *109*, 1663.
(9) (a) Diedenhofen, M.; Wagener, T. M.; Frenking, G. In *Computational Organometallic Chemistry*; Cundari, T. R., Ed.; Marcel Dekker: Basel, 2001; p 69. (b) Pierloot, K. In *Computational Organometallic Chemistry*; Cundari, T. R., Ed.; Marcel Dekker: Basel, 2001; p 123. (c) Frenking, G.; Fröhlich, N. *Chem. Rev.* **2000**, *100*, 717. (d) Frenking, G.; Wickmann, K.; Frölich, N.; Loschen, C.; Lein, M.; Funzke, J.; Rayón, V. M. *Coord. Chem. Rev.* **2003**, *238*, 55. (e) Morokuma, K. *J. Chem. Phys.* **1971**, *55*, 1236. (f) Kitaura, K.; Morokuma, K. *Int. J. Quantum Chem.* **1976**, *10*, 325. (g) Ziegler, T.; Rauk, A. *Theor. Chim. Acta* **1977**, *46*, 1. (h) Ziegler, T.; Rauk, A. *Inorg. Chem.* **1979**, *18*, 1558. (i) Bagus, P. S.; Hermann, K.; Bauschlicher, C. W. *J. Chem. Phys.* **1984**, *80*, 4378.
(10) Bartlett, R. J. *Annu. Rev. Phys. Chem.* **1981**, *32*, 359.
(11) Goddard, W. A.; Dunning, T. H.; Hunt, W. J.; Hay, P. J. *Acc. Chem. Res.* **1973**, *6*, 368.
(12) Ross, B. O. *Adv. Chem. Phys.* **1987**, *69*, 399.
(13) Andersson, K.; Malmqvist, P. Å.; Ross, B. O. *J. Chem. Phys.* **1992**, *96*, 1218.
(14) Kohn, W.; Sham, L. J. *Phys. Rev.* **1965**, *140*, A1133.
(15) (a) Koch, W.; Holthausen, M. C. *A Chemist's Guide to Density Functional Theory*; Wiley-VCH: Chichester, 2000. (b) Kohn, W.; Becke, A. D.; Parr, R. G. *J. Phys. Chem.* **1996**, *100*, 12974. (c) Parr, R. G.; Yang, W. *Density Functional Theory of the Electronic*

Structure of Molecules; Oxford University Press: New York, 1989. (d) Ziegler, T. *Chem. Rev.* **1991**, *91*, 651. (e) Laird, B. B., Ross, R., Ziegler, T., Eds. *Chemical Applications of Density Functional Theory*; American Chemical Society: Washington, DC, 1996, 1997.
(16) Hohenberg, P.; Kohn, W. *Phys. Rev.* **1964**, *136*, B864.
(17) (a) Becke, A. D. *J. Chem. Phys.* **1986**, *84*, 4524. (b) Becke, A. D. *J. Comput. Chem.* **1999**, *20*, 63. (c) Becke, A. D. *Phys. Rev.* **1988**, *38*, A3098. (d) Perdew, J. P.; Schmidt, K. In *Density Functional Theory and Its Application to Materials*; Van Doren, V., et al., Eds.; American Institute of Physics: Melville, NY, 2001.
(18) (a) Perdew, J. P. *Phys. Rev.* **1986**, *33*, B8822. (b) Perdew, J. P.; Burke, K.; Ernzerhof, M. *Phys. Rev. Lett.* **1996**, *77*, 3865.
(19) (a) Lee, C.; Yang, W.; Parr, R. G. *Phys. Rev.* **1988**, *37*, B785. (b) Zhang, Y.; Yang, W. *Phys. Rev. Lett.* **1998**, *80*, 890. (c) Hammer, B.; Hansen, L. B.; Nørskov, J. K. *Phys. Rev.* **1999**, *59*, 7413.
(20) (a) Becke, A. D.; Roussel, M. R. *Phys. Rev.* **1989**, *39*, A3761. (b) Tschinke, V.; Ziegler, T. *Can. J. Chem.* **1989**, *67*, 460. (c) Proynov, E.; Vela, A.; Salahub, D. R. *Chem. Phys. Lett.* **1994**, *230*, 419. (d) van Voorhis, T.; Scuseria, G. E. *Mol. Phys.* **1997**, *92*, 601. (e) Filitov, M.; Thiel, W. *Phys. Rev.* **1988**, *57*, A189. (e) Perdew, J. P.; Zunger, A. *Phys. Rev.* **1981**, *23*, B5048. (f) Patchkovskii, S.; Autschbach, J.; Ziegler, T. *J. Chem. Phys.* **2001**, *115*, 26. (g) Patchkovskii, S.; Ziegler, T. *J. Chem. Phys*. **2002**, *116*, 7806. (h) Baerends, E. J. *Phys. Rev. Lett.* **2001**, *87*, 133004. (i) Buijse, M. A.; Baerends, E. J. *Mol. Phys.* **2002**, *100*, 401. (i) Gritsenko, O. V.; Ensing, B.; Schipper, P. R. T.; Baerends, E. J. *J. Phys. Chem.* **2000**, *A104*, 8558. (j) Becke, A. D. *J. Chem. Phys.* **2003**, *117*, 6935. (k) Imamura, Y.; Scuseria, G. E.; Martin, R. M. *J. Chem. Phys.* **2002**, *116*, 6458. (l) Ernzerhof, M.; Scuseria, G. E. *J. Chem. Phys.* **1999**, *110*, 5029. (m) Tao, J.; Perdew, J. P.; Staroverov, V. N.; Scuseria, G. E. *J. Chem. Phys.* **2004**, *120*, 6890−6897.
(21) Becke, A. D. *J. Chem. Phys.* **1993**, *98*, 1372.
(22) Pulay, P. *Mol. Phys.* **1969**, *17*, 197.
(23) (a) Matveev, A.; Staufer, M.; Mayer, M.; Rösch, N. *Int. J. Quantum Chem.* **1999**, *75*, 863. (b) Bray, M. R.; Deeth, R. T. J.; Paget, V. J.; Sheen, P. D. *Int. J. Quantum Chem.* **1997**, *61*, 85. (c) Gonzalez, O.; Branchadell, V.; Monteyne, K.; Ziegler, T. *Inorg. Chem.* **1998**, *37*, 1744. (d) Fischer, J. M.; Piers, W. E.; Ziegler, T.; MacGillivray, L. R.; Zaworotko, M. J. *Chem. Eur. J.* **1996**, *2*, 120. (e) Pietsch, M. A.; Couty, M.; Hall, M. B. *J. Phys. Chem.* **1995**, *99*, 16315. (f) Thomas, J. L. C.; Hall, M. B. *Organometallics* **1997**, *16*, 2318. (g) Niu, S.; Hall, M. B. *J. Phys. Chem A* **1977**, *101*, 1360. (h) Büjse, M. A.; Baerends, E. J. *J. Chem. Phys.* **1989**, *93*, 4129. (i) Sandblom, N.; Chivers, T.; Ziegler, T. *Can. J. Chem.* **1996**, *74*, 2363.
(24) Ziegler, T. In *Computational Thermochemistry*; Irikura, K. K., Frurip, D. J., Eds.; ACS Symposium Series 677; American Chemical Society: Washington, DC, 1999; pp 369.
(25) . Blomberg, M. R. A.; Siegbahn, P. E. M. In *Computational Thermochemistry*; Irikura, K. K., Frurip, D. J., Eds.; ACS Symposium Series 677; American Chemical Society: Washington, DC, 1999; pp 197.
(26) (a) Pyykkö, P. *Chem. Rev.* **1988**, *88*, 563. (b) B. A. In *Encyclopedia of Computational Chemistry*; Schleyer, P. v. R., Ed.; John Wiley & Sons: Chichester, 1998; pp 2499. (c) Kaltsoyannis, N. *J. Chem. Soc., Dalton Trans.* **1997**, *1*.
(27) (a) Ziegler, T.; Snijders, J. G.; Baerends, E. J. In *The Challenge of d and f Electrons*; Salahub, D. R., Zerner, M., Eds.; ACS Symposium Series 394; American Chemical Society: Washington, DC, 1989; p 322. (b) Jian, L.; Schreckenbach, G.; Ziegler, T. *J. Am. Chem. Soc.* **1995**, *117*, 486. (c) Ziegler, T. *Can. J. Chem*. **1995**, *73*, 743.
(28) Li, J.; Ziegler, T. *Inorg. Chem.* **1995**, *34*, 3245.
(29) (a) Ziegler, T.; Snijders, J. G; Baerends, E. J. *J. Chem. Phys.* **1981**, *74*, 1271. (b) Autschbach, J.; Schwarz, W. H. E. *Theor. Chem. Acc.* **2000**, *104*, 82.
(30) Wezenbeek, E. M.; Baerends, E. J.; Ziegler, T. *Inorg. Chem.* **1995**, *34*, 238.
(31) (a) Nakamoto, K. *Infrared and Raman Spectra of Inorganic and Coordination Compounds*, 4th ed.; John Wiley & Sons: New York, 1986. (b) Wilson, E. B., Jr.; Decius, J. C.; Cross P. C. *Molecular Vibrations*; McGraw-Hill: New York, 1955. (c) Gerratt, J.; Mills, I. M. *J. Chem. Phys.* **1966**, *44*, 2480. (d) Pople, J. A.; Krishan, R.; Schlegel, H. B.; Binkley, J. S. *Int. J. Quantum Chem*. **1979**, *S13*, 225. (e) Scott, A. P.; Radom, L. *J. Phys. Chem.* **1996**, *100*, 16502. (f) Jonas, V.; Thiel, W. J. *Chem. Phys.* **1995**, *102*, 8474. (g) Berces, A.; Ziegler, T. *Top. Curr. Chem.* **1996**, *182*, 42. (h) Heidrich, D. In *The Reaction Path in Chemistry*; Heidrich, D., Ed.; Kluwer Academic Publishers: Norwell, MA, 1995; p 1.
(32) (a) Ionova, I. V.; Carter, E. A. *J. Chem. Phys*. **1994**, *10*, 6562. (b) Ulitsky, A.; Elber, R. J. *J. Chem. Phys.* **1990**, *92*, 1510. (c) Sandre, E.; Payne, M. C.; Stich, I.; Gale, J. D. In *Transition State Modeling for Catalysis*; Truhlar, D. G., Morokuma, K., Eds.; ACS Symposium Series 721; American Chemical Society: Washington, DC, 1999; p 346. (d) Banerjee, A.; Adams, N.; Simons, J.; Shepard, R. *J. Phys. Chem.* **1985**, *89*, 52. (e) Baker, J. *J. Comput. Chem.* **1986**, *7*, 385.
(33) (a) Fukui, K. *Acct. Chem. Res.* **1981**, *14*, 363. (b) Tachibana, A.; Fukui, K. *Theor. Chem. Acta*, **1980**, *57*, 81. (c) Fukui, K. *Int. J. Quantum Chem. Symp.* **1981**, *15*, 633. (d) Hratchian, H. P.; Schlegel, H. B. *J. Chem. Phys.* **2004**, *120*, 9918−9924.
(34) Johnson, L. K.; Mecking, S.; Brookhart, M. *J. Am. Chem. Soc.* **1996**, *118*, 267.
(35) Yang, W.; Lee, T.-S. *J. Chem. Phys.* **1995**, *103*, 5674.
(36) (a) Warshel, A.; Levitt, M. *J. Mol. Biol*. **1976**, *103*, 227. (b) Singh, U. C.; Kollman, P. A. *J. Comput. Chem.* **1986**, *7*, 718. (c) Field, M.; Bash, P. A.; Karplus, M. *J. Comput. Chem.* **1990**, *11*, 700. (d) Maseras, F.; Morokuma, K. *J. Comput. Chem.* **1995**, *16*, 1170. (e) Woo, T. K.; Cavello, L.; Ziegler, T. *Theor. Chem. Acc.* **1998**, *100*, 307.
(37) (a) Maseras, F. In *Computational Organometallic Chemistry*; Cundari, T. R., Ed.; Marcel Dekker: Basel, 2001; p 159. (b) Deng, L.; Woo, T. K.; Margl, P. M.; Ziegler, T. *J. Am. Chem. Soc.* **1997**, *119*, 6177. (c) Svensson, M.; Humbel, S.; Froese, R. D. J.; Matsubara, T.; Sieber, S.; Morokuma, K. *J. Phys. Chem.* **1996**, *100*, 19357. (d) Bakowies, W.; Thiel, D. *J. Phys. Chem.* **1996**, *100*, 10580. (e) Comba, P.; Hambley, T. W. *Molecular Modeling of Inorganic Compounds*, 2nd ed.; Wiley-VCH: New York, 2001.
(38) Tapia, O.; Bertrán, J. *Solvent Effects and Chemical Reactivity*; Kluwer: Dordrecht, 1996.
(39) Klamt, A.; Schuurmann, G. *J. Chem. Soc., Perkin Trans.* **1993**, *2*, 799.
(40) (a) Cramer, C. J.; Truhlar, D. G. In *Reviews in Computational Chemistry*; Lipkowitz, K. B., Boyd, D. B., Eds.; VCH Publishers: New York, 1995; Vol. 6. (b) Pye, C.; Ziegler, T. *Theor. Chem. Acc.* **1999**, *101*, 396.
(41) (a) Tomasi, J. *Chem. Rev.* **1994**, *94*, 2027. (b) Kovalenko, A.; Hirata, F. *J. Chem. Phys.* **2000**, *112*, 10391.
(42) Surface dipoles and other more complicated schemes can be envisioned.
(43) Gao, J. In *Reviews in Computational Chemistry*; Lipkowitz, K. B., Boyd, D. B., Eds.; VCH: New York, 1996; Vol. 7.
(44) Car, R.; Parrinello, M. *Phys. Rev. Lett.* **1985**, *55*, 2471.
(45) Curioni, A.; Sprik, M.; Andreoni, W.; Schiffer, H.; Hutter, J.; Parrinello, M. M. *J. Am. Chem. Soc.* **1997**, *119*, 7218.
(46) Tuckerman, M. E.; Lasonen, K.; Sprik, M.; Parrinello, M. *J. Phys. Chem.* **1995**, *99*, 5749.
(47) Gao, J. *Acc. Chem. Res.* **1992**, *29*, 298.
(48) Woo, T. K.; Blöchl, P. E.; Ziegler, T. *J. Mol. Struct.: THEOCHEM* **2000**, *506*, 313−334.
(49) Solomon, E. I., Lever, A. B. P., Eds. *Inorganic Electronic Structure and Spectroscopy*; Wiley: New York, 1999; Vol. I−II.
(50) van Gisbergen, S. J. A.; Groeneveld, J. A.; Rosa, A.; Snijders, J. G.; Baerends, E. J. *J. Phys. Chem. A* **1999**, *103*, 6835.
(51) Nakai, H.; Ohmori, Y.; Nakatsuji, H. *J. Chem. Phys.* **1991**, *95*, 8287.
(52) (a) Ziegler, T.; Rauk, A.; Baerends, E. J. *Theor. Chim. Acta* **1977**, *43*, 261. (b) Daul, C. *Int. J. Quantum Chem.* **1994**, *52*, 867.
(53) Slater, J. C. *Adv. Quantum Chem.* **1972**, *6*, 1.
(54) (a) Petersilka, M.; Grossmann, U. J.; Gross, E. K. U. *Phys. Rev. Lett*. **1996**, *76*, 12. (b) Jamorski, C.; Casida, M. E.; Salahub, D. R. *J. Chem. Phys.* **1996**, *104*, 5134. (c) van Gisbergen, S. J. A.; Snijders, J. G.; Baerends, E. J. *J. Chem. Phys.* **1995**, *103*, 9347. (d) Runge, E.; Gross, E. K. U. *Phys. Rev.* **1980**, *21*, A1561. (e) van Caillie, C.; Amos, R. D. *Chem. Phys. Lett.* **1998**, *291*, 71.
(55) (a) Ziegler, T.; Rauk, A.; Baerends, E. J. *J. Chem. Phys.* **1976**, *16*, 209. (b) Stückl, A.; Daul, C. A.; Güdel, H. U. *J. Chem. Phys.* **1997**, *107*, 4606. (c) Roos, B. O. *Acc. Chem. Res*. **1999**, *32*, 137.
(56) van Gisbergen, S. J. A.; Fonseca Guerra, C.; Baerends, E. J. *J. Comput. Chem.* **2000**, *21*, 1511.
(57) Kaupp, M., Bühl, M., Malkin, V. G., Eds. *Calculation of NMR and EPR Parameters*; Wiley-VCH: Weinheim, 2004.
(58) Autschbach, J.; Ziegler, T. *Coord. Chem. Rev*. **2003**, *238*, 83−126.
(59) Autschbach, J.; Ziegler, T. In *Encyclopedia of Nuclear Magnetic Resonance*; Grant, D. M., Harris, R. K., Eds.; Wiley: Chichester, 2002; Vol. 9.
(60) Patchkovskii, S.; Autschbach, J.; Ziegler, T. *J. Chem. Phys*. **2001**, *115*, 26.
(61) Gauss, J.; Stanton, J. F. In *Calculation of NMR and EPR Parameters*; Kaupp, M., Bühl, M., Malkin, V. G., Eds.; Wiley-VCH: Weinheim, 2004; pp 123−137.
(62) (a) Schreckenbach, G.; Ziegler, T. *Int. J. Quantum Chem.* **1997**, *61*, 899−918. (b) Kaupp, M.; Malkin, O. L.; Malkina, O. L. *J. Am. Chem. Soc.* **1995**, *117*, 8492. (c) Autschbach, J. The calculation of NMR parameters in transition metal complexes. In *Density Functional Theory in Inorganic Chemistry, Series Structure and Bonding*; Kaltsoyannis, N., McGrady, J. E., Eds.; Springer: Heidelberg, 2004; Vol. 112, pp 1−48.
(63) Wolff, S. K.; Ziegler, T. *J. Chem. Phys*. **1998**, *109*, 895−905.
(64) Namura, Y.; Takeuchi, Y.; Nagakawa, N. *Tetrahedron Lett*. **1969**, *8*, 639.
(65) Wolff, S. K.; Ziegler, T.; van Lenthe, E.; Baerends, E. J. *J. Chem. Phys.* **1999**, *110*, 7689−7698.

(66) Helgakar, T.; Pecul, M. In *Calculation of NMR and EPR Parameters*; Kaupp, M., Bühl, M., Malkin, V. G., Eds.; Wiley-VCH: Weinheim, 2004; pp 101−121.
(67) Khandogin, J.; Ziegler, T. *Spectrochim. Acta* **1999**, *55*, 607.
(68) Autschbach, J.; Ziegler, T. *J. Chem. Phys.* **2002**, *116*, 891−896.
(69) Autschbach, J.; Ziegler, T. *J. Am. Chem. Soc*. **2001**, *123*, 3341.
(70) Autschbach, J.; Ziegler, T. In *Calculation of NMR and EPR Parameters*; Kaupp, M., Bühl, M., Malkin, V. G., Eds.; Wiley-VCH: Weinheim, 2004; pp 249−262.
(71) (a) Neese, F. J. *Chem. Phys*. **2001**, *115*, 11080. (b) Schreckenbach, G.; Patchkovskii, S. In *Calculation of NMR and EPR Parameters*; Kaupp, M., Bühl, M., Malkin, V. G., Eds.; Wiley-VCH: Weinheim, 2004; pp 505−530. (c) Patchkovskii, S.; Autschbach, J.; Ziegler, T. *J. Chem. Phys*. **2001**, *115*, 26. (d) Kaupp, M. In *EPR Spectroscopy of Free Radicals in Solids. Trends in Methods and Applications*; Lund, A., Shiotani, M., Eds.; Kluwer: Dordrecht, 2002. (e) Lushington, G. H. *J. Phys. Chem. A* **2000**, *104*, 2969.
(72) Patchkovskii, S.; Ziegler, T. *J. Chem. Phys.* **1999**, *111*, 5730.
(73) Malkina, O. L.; Malkin, V. *J. Am. Chem. Soc*. **2000**, *122*, 9206.
(74) Patchkovskii, S.; Ziegler, T. *J. Am. Chem. Soc.* **2000**, *122*, 3506.
(75) van Lenthe, E.; van der Avoird, A.; Hagen, W. R.; Reijerse, E. J. *J. Phys. Chem. A* **2000**, *104*, 2070.
(76) Wanner, M.; Scheiring, T.; Kaim, W. *Inorg. Chem.* **2001**, *40*, 5704.
(77) Stein, M; van Lenthe, E.; Baerends, E. J.; Lubitz, W. *J. Phys. Chem. A* **2001**, *105*, 416.
(78) (a) Harriman, J. E. *Theoretical Foundations of Electron Spin Resonance*; Academic Press: New York, 1978. (b) Abragam, A.; Bleany, B. *Electron Paramagnetic Resonance for Transition Ions*; Clarendon Press: Oxford, 1970.
(79) Eriksson, L. A. ESR hyperfine calculations. In *Encyclopedia of Computational Chemistry*; von Ragu'e Schleyer, P., Ed.; Wiley: Chichester, 1998; pp 952−958.
(80) Munzarov'a, M.; Kaupp, M. *J. Phys. Chem. A* **1999**, *103*, 9966.
(81) Schlegel, H. B. Spin contamination. In *Encyclopedia of Computational Chemistry*; von Ragu'e Schleyer, P., Ed.; Wiley: Chichester, 1998; pp 2665−2671.
(82) Munzarov'a, M. L.; Kubacek, P.; Kaupp, M. *J. Am. Chem. Soc.* **2000**, *121*, 11900.
(83) Belanzoni, P.; van Lenthe, E.; Baerends, E. J. *J. Chem. Phys*. **2001**, *114*, 4421.
(84) (a) Belanzoni, P.; Baerends, E. J.; van Asselt, S.; Langeven, P. B. *J. Phys. Chem.* **1995**, *99*, 13094. (b) Belanzoni, P.; Baerends, E. J.; Gribnau, M. *J. Phys. Chem. A* **1999**, *103*, 3732.
(85) (a) Jonas, V.; Thiel, W. *J. Chem. Phys.* **1995**, *102*, 8474. (b) Jonas, V.; Thiel, W. *Organometallics* **1998**, *17*, 353. (c) Jonas, V.; Thiel, W. *J. Phys. Chem. A* **1999**, *103*, 1381.
(86) Koch, W.; Holthausen, M. C. *A Chemist's Guide to Density Functional Theory*; VCH: Weinheim, 2000.
(87) Amos, R. D. *Adv. Chem. Phys*. **1987**, *67*, 99.
(88) Wilson, E. B., Jr.; Decious, J. P.; Cross, P. C. *Molecular Vibrations. The Theory of Infrared and Raman Vibrational Spectra*; McGraw-Hill: New York, 1955.
(89) Hay, P. J.; Martin, R. L. *J. Chem. Phys.* **1998**, *109*, 3875.
(90) Fan, L.; Ziegler, T. *J. Chem. Phys*. **1992**, *96*, 9005.
(91) Diaz-Acosta, I.; Baker, J.; Cordes, W.; Pulay, P. *J. Phys. Chem.* **2001**, *A105*, 238.
(92) Jarzecki, A. A.; Kozlowski, P. M.; Pulay, P.; Ye, B.-H.; Li, X.-Y. *Spectrochim. Acta* **1997**, *A53*, 1195.
(93) Kozlowski, P. M. *J. Phys. Chem. A* **1999**, *103*, 1357.
(94) Pulay, P. J. *Mol. Struct.* **1996**, 347.
(95) Pulay, P. Analytical derivative techniques and the calculation of vibrational spectra. In *Modern Electronic Structure Theory Part II*; Yarkony, D. R., Ed.; World Scientific: River Edge, NJ, 1995; Vol. 2, pp 1191−1240.
(96) McClain, B. L.; Clark, S. M.; Gabriel, R. L.; Ben-Amotz, D. J. *Chem. Educ*. **2000**, *77*, 654.
(97) (a) Nafie, L. A.; Freedman, T. B. *J. Phys. Chem*. **1983**, *78*, 7108. (b) Stephens, P. J. *J. Phys. Chem.* **1985**, *89*, 748. (c) Nafie, L. A. *J. Chem. Phys.* **1992**, *718*, 96.
(98) Yang D.; Rauk, A. *J. Chem. Phys.* **1994**, *100*, 7995.
(99) Stephens, P. J.; Chabalowski, C. F.; Devlin, F. J.; Jalkanen, K. J. *Chem. Phys. Lett.* **1994**, *225*, 247.
(100) Bak, K. L.; Jørgensen, P.; Helgaker, T.; Ruud, K.; Jensen, H. J. A. *J. Chem. Phys.* **1993**, *98*, 8873.
(101) He, Y.; Cao, Y.; Nafie, L. A.; Freedman, T. A. *J. Am. Chem. Soc.* **2001**, *120*, 231.
(102) Charney, E. *The Molecular Basis of Optical Activity*; John Wiley & Sons Ltd.: New York, 1979.
(103) (a) Condon, E. U. *Rev. Mod. Phys.* **1937**, *432*, 9. (b) Moscowitz, A. *Adv. Chem. Phys*. **1962**, *4*, 67. (c) Charney, E. *The Molecular Basis of Optical Activity*; John Wiley & Sons Ltd.: New York, 1979.
(104) (a) Grimme, S. *Chem. Phys. Lett*. **2001**, *339*, 380. (b) Yabana, K.; Bertsch, G. F. *Phys. Rev. A* **1999**, *60*, 1271. (c) Furche, F. *J. Am. Chem. Soc.* **2000**, *122*, 1717. (d) Cheeseman, J. R.; Frisch, M. J.; Devlin, F. J.; Stephens, P. J. *J. Phys. Chem. A* **2000**, *104*, 1039. (e) Polavarapu, P. L.; Chakraborty, D. K.; Ruud, K. *Chem. Phys. Lett.* **2000**, *319*, 595. (f) Stephens, P. J. *Tetrahedron: Asymmetry* **2000**, *11*, 2443. (g) Furche, F.; Ahlrichs, R. *J. Chem. Phys.* **2001**, *114*, 10362. (h) Autschbach, J.; Ziegler, T. *J. Chem. Phys.* **2002**, *116*, 891. (h) Autschbach, J.; Ziegler, T.; van Gisbergen, S. J. A.; Baerends, E. J. *J. Chem. Phys.* **2002**, *6930*, 116. (i) Autschbach, J.; Ziegler, T.; Patchkovskii, S.; van Gisbergen, S. J. A.; Baerends, E. J. *J. Chem. Phys*. **2002**, *116*, 581. (j) Grimme, S.; Waletzke, M. J. *Chem. Phys*. **1999**, *111*, 5645. (k) Ruud, K.; Helgaker, T. *Chem. Phys. Lett.* **2002**, *352*, 533.
(105) Kuroda, R.; Saito, Y. Circular dichroism of inorganic complexes. Nakanishi, K., Berova, N., Woody, R. W., Eds. *Circular Dichroism: Principles and Applications*; VCH Publishers Inc.: New York, 1994.
(106) Volosov, A.; Woody, A. W. Theoretical approach to natural electronicoptical activity. In *Circular Dichroism: Principles and Applications*; Nakanishi, K., Berova, N., Woody, R. V., Eds.; VCH: New York, 1994.
(107) (a) Kuroda, R.; Saito, R. Circular dichroism of inorganic complexes: Interpretation and applications. In *Circular Dichroism: Principles and Applications*; Nakanishi, K., Berova, N., Woody, R. W., Eds.; VCH: New York, 1994. (b) Ballhausen, C. J. *Molecular Electronic Structures of TransitionMetal Complexes*; McGraw-Hill: London, 1979. (c) Mason, S. F. Optical activity an molecular dissymmetry in coordination compounds. In *Fundamental Aspects and Recent Developments in Optical Rotatory Dispersion and Circular Dichroism*; Ciardelli, F., Salvatory, P., Eds.; Heyden and Son Ltd.: London, 1973.
(108) (a) *Stereochemistry of Optically Active Transition Metal Compounds*; Douglas, B. E., Saito, Y., Eds.; ACS Symposium Series 119; Americal Chemical Society: Washington, DC, 1980. (b) Mason, S. F.; Peart, B. J. *J. Chem. Soc., Dalton Trans*. 1977, 937.
(109) (a) Autschbach, J.; Jorge, F. E.; Ziegler, T. *Inorg. Chem*. **2003**, *42*, 2867. (b) Jorge, F. E.; Autschbach, J.; Ziegler, T. *Inorg. Chem*. **2003**, *42*, 8902. (c) Jorge, F. E.; Autschbach, J.; Ziegler, T. *J. Am. Chem. Soc*. Accepted for publication. (d) Le Guennic, B.; Hieringer, W.; Goerling, A.; Autschbach, J. Submitted for publication.
(110) Faraday, M. *Philos. Mag.* **1846**, *28*, 294.
(111) (a) Buckingham, A. D.; Stephens, P. J. *Annu. Rev. Phys. Chem.* **1966**, *17*, 399. (b) Stephens, P. J. *Annu. Rev. Phys. Chem.* **1974**, *25*, 201. (c) Stephens, P. J. *Adv. Chem. Phys.* **1976**, *35*, 197.
(112) Solomon, E. L.; Pavel, E. G.; Loeb, K. E.; Campochiaro, C. *Coord. Chem. Rev.* **1995**, *144*, 369.
(113) (a) Fleischhauer, J.; Michl, J. *J. Phys. Chem. A* **2000**, *104*, 7776. (b) Michl, J. *Tetrahedron* **1984**, *40*, 3845.
(114) (a) Bishop, D. M.; Cybulski, C. M. *J. Chem. Phys*. **1990**, *93*, 590. (b) Coriani, S.; Jorgensen, P.; Christiansen, O.; Gauss, J. *Chem. Phys. Lett*. **2000**, *330*, 463.
(115) (a) Banerjee, A.; van Gisbergen, S. J. A.; Autschbach, J.; Baerends, E. J.; Ziegler, T. *Int. J. Quantum Chem*. In press. (b) Krykunov, M.; Banerjee, A.; Ziegler, T.; Autschbach, J. *J. Chem. Phys*. **2005**, *122*, 074105.
(116) Seth, M.; Ziegler, T.; Banerjee, A.; Autschbach, J.; van Gisbergen, S. J. A.; Baerends, E. J. *J. Chem. Phys.* **2004**, *120*, 10942.
(117) Seth, M; Autschbach, J.; Ziegler, T. *J. Chem. Phys*. Submitted for publication.
(118) Levine, R. D.; Bernstein, R. B. *Molecular Reaction Dynamics*; Clarendon Press: Oxford, 1974.
(119) Truhlar, D. G., Ed. *Potential Energy Surfaces and Dynamics Calculations*; Plenum: New York, 1981.
(120) Sato, S. *J. Chem. Phys.* **1955**, *23*, 592.
(121) Rappé, A. K.; Pietsch, M. A.; Wiser, D. C.; Hart, J. R.; Bormann, L. M.; Skiff, W. M. *J. Mol. Eng.* **1997**, *7*, 385.
(122) Schatz, G. C. In *Advances in Molecular Electronic Structure Theory*; Dunning, T. H., Jr., Ed.; JAI Press Inc.: Greenwich, CT, 1990; p 85.
(123) Harding, L. B. In *Advances in Molecular Electronic Structure Theory*; Dunning, T. H., Jr., Ed.; JAI Press Inc.: Greenwich, CT, 1990; p 45.
(124) Corchado, J. C.; Truhlar, D. G. In *Combined Quantum Mechanical and Molecular Mechanical Methods*; Gao, J., Thompson, M. A., Eds.; ACS Symposium Series 712; American Chemical Society: Washington, DC, 1998; pp 106.
(125) Gordon, M. S.; Chaban, G.; Taketsugu, T. *J. Phys. Chem.* **1996**, *100*, 11512.
(126) (a) Liu, J.; Song, K.; Hase, W. L.; Anderson, S. L. *J. Am. Chem. Soc*. **2004**, *126*, 8602. (b) Liu, J.; Li, Z.; Dai, Z.; Huang, X.; Sun, C. *J. Chem. Phys. A* **2003**, *107*, 6231.
(127) Worth, G. A.; Hunt, P.; Robb, M. A. *J. Phys. Chem. A* **2003**, *107*, 621.
(128) Paterson, M. J.; Hunt, P. A.; Robb, M. A.; Takahashi, O. *J. Phys. Chem. A*. **2002**, *106*, 10494.
(129) Schlegel, H. B. *Bull. Kor. Chem. Soc.* **2003**, *24*, 837−842.
(130) Miller, W. H.; Handy, N.; Adams, J. E. *J. Chem. Phys.* **1980**, *72*, 99.
(131) Kraka, E.; Dunning, T. H., Jr. In *Advances in Molecular Electronic Structure Theory*; Dunning, T. H., Jr., Ed.; JAI Press Inc.: Greenwich, CT, 1990; p 129.
(132) Car, R.; Parrinello, M. *Phys. Rev. Lett.* **1985**, *55*, 2471.

(133) (a) Aagaard, O. M.; Meier, R. J.; Buda, F. *J. Am. Chem. Soc.* **1998**, *120*, 7174. (b) Senn, H. M.; Blöchl, P. E.; Togni, A. *J. Am. Chem. Soc.* **2000**, *122*, 4098. (c) De Angelis, F.; Sgamellotti, A.; Re, N. *Organometallics* **2000**, *19*, 4104.
(134) Woo, T. K.; Blöchl, P. E.; Ziegler, T. *J. Phys. Chem A* **2000**, *104*, 121.
(135) (a) De Angelis, F.; Sgamellotti, A.; Rega, N.; Cossi, M.; Barone, V. *Chem. Phys. Lett.* **2000**, *328*, 302. (b) Fattebert, J.-L.; Gygi, F. *J. Comput. Phys.* **2002**, *23*, 662. (c) Senn, H. M.; Margl, P. M.; Schmid, R.; Ziegler, T.; Blöchl, P. E. *J. Chem. Phys.* **2003**, *118*, 1089.
(136) VandeVondele, J.; Hutter, J. *J. Chem. Phys.* **2003**, *118*, 4365.
(137) (a) Pijper, E.; Kroes, G. J.; Olsen, R. A.; Baerends, E. J. *J. Chem. Phys.* **2000**, *113*, 8300. (b) Jarid, A.; Moreno, M.; Lledos, A.; Lluch, J. M.; Bertran, J. *J. Am. Chem. Soc.* **1993**, *115*, 5861. (c) Heitz, M.-C.; Daniel, C. *J. Am. Chem. Soc.* **1997**, *119*, 8269. (d) Guillaumont, D.; Daniel, C. *J. Am. Chem. Soc.* **1999**, *121*, 11733. (e) Maseras, F.; Lledós, A.; Clot, E.; Eisenstein, O. *Chem. Rev.* **2000**, *100*, 601.
(138) (a) Hehre, W. J.; Radom, L.; Schleyer, P. v. R.; Pople, J. A. *Ab Initio Molecular Orbital Theory*; Wiley: New York, 1986. (b) Garrett, B. C.; Truhlar, D. G. *J. Chem. Phys.* **1979**, *70*, 1593.
(139) Baker; Muir, J. M.; Andzelm, J. *J. Chem. Phys.* **1995**, *102*, 2063.
(140) (a) Bauschlicher, C. W.; Maitre, P. *Chem. Phys. Lett.* **1996**, *246*, 40. (b) Siegbahn, P. E. M. *Adv. Chem. Phys.* **1996**, *XCIII*. (c) Harrison, J. F. *Chem. Rev*. **2000**, *100*, 679.
(141) (a) Rotzinger, F. P. *J. Am. Chem. Soc*. **1997**, *119*, 5230. (b) De Vito, D.; Sidorenkova, H.; Rotzinger, F. P.; Weber, J.; Merbach, A. E. *Inorg. Chem.* **2000**, *39*, 5547.
(142) (a) Deeth, R. J.; Elding, L. I. *Inorg. Chem.* **1996**, *35*, 5019. (b) Lin, Z.; Hall, M. B. *Inorg. Chem.* **1991**, *30*, 646.
(143) (a) Han, Y.; Deng, L.; Ziegler, T. *J. Am. Chem. Soc.* **1997**, *119*, 5939.
(144) Wang, W.; Weitz, E. *J. Phys. Chem.* **1997**, *101*, 2358. (b) Musaev, D.; Morokuma, K. *J. Am. Chem. Soc.* **1995**, *117*, 799.
(145) (a) Niu, S.; Hall, M. B. *Chem. Rev.* **2000**, *100*, 353. (b) Dedieu, A. *Chem. Rev.* **2000**, *100*, 543.
(146) (a) Margl, P.; Deng, L.; Ziegler, T. *J. Am. Chem. Soc*. **1998**, *120*, 5517. (b) Krogh-Jespersen, K.; Goldman, A. S. In *Transition State Modeling for Catalysis*; Truhlar, D. G., Morokuma, K., Eds.; ACS Symposium Series 721; American Chemical Society: Washington, DC, 1999; pp 151. (c) Wu, Y. D.; Peng, Z.-H. In *Transition State Modeling for Catalysis*; Truhlar, D. G., Morokuma, K., Eds.; ACS Symposium Series 721; American Chemical Society: Washington, DC, 1999; pp 151. (d) Folga, E.; Woo, T. K.; Ziegler, T. In *Theoretical Aspects of Homogeneous Catalysis*; van Leeuwen, P. W. N. M., Ed.; Kluwer Academic Publishers: Dordrecht, 1995; p 115.
(147) (a) Mavrikakis, M.; Hansen, L. B.; Mortensen, J. J.; Hammer, B.; Nørskov, J. K. In *Transition State Modeling for Catalysis*; Truhlar, D. G., Morokuma, K., Eds.; ACS Symposium Series 721; American Chemical Society: Washington, DC, 1999; p 245. (b) Neurock, M.; Pallassana, V. In *Transition State Modeling for Catalysis*; Truhlar, D. G., Morokuma, K., Eds.; ACS Symposium Series 721; American Chemical Society: Washington, DC, 1999; p 226. (c) Witten, J. L.; Yang, H. In *Transition State Modeling for Catalysis*; Truhlar, D. G., Morokuma, K., Eds.; ACS Symposium Series 721; American Chemical Society: Washington, DC, 1999; pp 274.
(148) (a) Torrent, M.; Sola, M.; Frenking, G. *Chem. Rev.* **2000**, *100*, 439. (b) Blaszkowski, S. A.; van Santen, R. A. in *Transition State Modeling for Catalysis*; Truhlar, D. G., Morokuma, K., Eds.; ACS Symposium Series 721; American Chemical Society: Washington, DC, 1999; p 307. (c) Sauer, J.; Sierka, M.; Haase, F. In *Transition State Modeling for Catalysis*; Truhlar, D. G., Morokuma, K., Eds.; ACS Symposium Series 721; American Chemical Society: Washington, DC, 1999; p 358. (d) Friesner, R. A.; Dunietz, B. D. **2001**, *34*, 351. (e) Siegbahn, P. E. M.; Blomberg, M. R. A. *Chem. Rev*. **2000**, *100*, 421. (f) Loew, G. H.; Harris, D. L. *Chem. Rev*. **2000**, *100*, 42.
(149) Truhlar, D. G.; Garrett, B. C. *Annu. Rev. Phys. Chem.* **1984**, *35*, 159.
(150) Beveridge, D. L.; DiCapua, F. M. *Annu. Rev. Biophys. Chem.* **1989**, *18*, 431.
(151) (a) Carter, E. A.; Ciccotti, G.; Hynes, J. T.; Kapral, R. *Chem. Phys. Lett.* **1989**, *156*, 472. (b) Paci, E.; Ciccotti, G.; Ferrario, G. M.; Kapral, R. *Chem. Phys. Lett.* **1991**, *176*, 581.
(152) (a) Margl, P.; Ziegler, T.; Blöchl, P. *J. Am. Chem. Soc.* **1995**, *117*, 12625. (b) Margl, P.; Ziegler, T.; Blöchl, P. E. *J. Am. Chem. Soc.* **1996**, *118*, 5412. (c) Margl, P.; Lohrenz, J. C. W.; Ziegler, T.; Blöchl, P. *J. Am. Chem. Soc.* **1996**, *118*, 4434. (d) Woo, T. K.; Margl, P. M.; Blöchl, P. E.; Ziegler, T. *J. Am. Chem. Soc.* **1996**, *118*, 13021. (e) Woo, T. K.; Margl, P.; Ziegler, T. *Organometallics* **1997**, *16*, 3454−3468. (f) Margl, P. M.; Woo, T. K.; Blöchl, P. E.; Ziegler, T. *J. Am. Chem. Soc.* **1998**, *120*, 2174−2175. (g) Woo, T. K.; Blöchl, P. E.; Ziegler, T. *J. Phys. Chem A* **2000**, *104*, 121−129. (h) Woo, T. K.; Margl, P. M.; Deng, L.; Ziegler, T. *Combined Quantum Mechanical and Molecular Mechanical Methods*; ACS Symposium Series 712; Gao, J., Thompson, M. A., Eds.; American Chemical Society: Washington, DC, 1998; pp 128−148. (i) Woo, T. K.; Margl, P. M.; Deng, L.; Cavallo, L.; Ziegler, T. *Transition State Modeling for Catalysis*; ACS Symposium Series 721; Truhlar, D. G., Morokuma, K., Eds.; American Chemical Society: Washington, DC, 1999; pp 173−187. (j) Woo, T. K.; Margl, P. M.; Deng, L.; Cavallo, L.; Ziegler, T. *Catal. Today* **1999**, *50*, 479.
(153) (a) Ensing, B.; Meijer, E. J.; Blöchl, P. E.; Baerends, E. J. *J. Phys. Chem A* **2001**, *105*, 3300. (b) Woo, T. K.; Blöchl, P. E.; Ziegler, T. *J. Mol. Struct.: THEOCHEM* **2000**, *506*, 313.
(154) (a) Kelly, E.; Seth, M.; Ziegler, T. *J. Phys. Chem. A* **2004**, *108*, 2167. (b) Yang, S. Y.; Hristov, I.; Fleurat-Lessard, P.; Ziegler, T. *J. Phys. Chem.* Submitted for publication.
(155) Rasmussen, T.; Jensen, J. F.; Ostergaard, N.; Tanner, D.; Ziegler, T.; Norrby, P.-O. *Chem. Eur. J.* **2002**, *8*, 177.
(156) Yang, S. Y.; Hristov, I.; Fleurat-Lessard, P.; Ziegler, T. *J. Phys. Chem*. **2005**, *109*, 197.
(157) Fleurat-Lessard, P.; Ziegler, T. *J. Chem. Phys*. Accepted for publication.
(158) Hirata, F.; Sato, H.; Ten-no, S.; Kato, S. In *Combined Quantum Mechanical and Molecular Mechanical Methods*; Gao, J., Thompson, M. A., Eds.; ACS Symposium Series 712; American Chemical Society: Washington, DC, 1998; p 188.
(159) (a) Tully, J. C. *Faraday Discuss.* **1998**, *110*, 407. (b) Garavelli, M.; Bernardi, F.; Olivucci, M.; Vreven, T.; Celani, P.; Robb, M. A. *Faraday Discuss*. **1998**, *110*, 51. (c) Truhlar, D. G. *Faraday Discuss.* **1998**, *110*, 521.

CR0307188